

**Sexual dimorphism in the dorsal root ganglia of neonatal mice identified by protein
expression profiling with single-cell mass cytometry**

Shayla Allis (Clark) Vradenburgh

Orlando, Florida

B.S. Psychology – Behavioral and Cognitive Psychology

University of Florida, 2017

A dissertation presented to the School of Medicine faculty of the University of Virginia in
candidacy for the degree of Doctorate in Philosophy

Department of Neuroscience

University of Virginia

April 2023

Table of Contents

Acknowledgments	3
Abstract	6
Chapter 1: Introduction to The Somatosensory Nervous System	7
1.1 Somatosensory Neurons	8
1.1.1 <i>Proprioceptors</i>	8
1.1.2 <i>Low Threshold Mechanoreceptors</i>	9
1.1.3 <i>Nociceptors</i>	10
1.2 Glial Cell Development in the Periphery	11
1.2.1 <i>Schwann Cells</i>	11
1.2.2 <i>Satellite Glial Cells</i>	12
1.3 Single-Cell Analysis in the DRG	15
1.4 Molecular and Functional Sexual Dimorphism in Somatosensory Cell Populations	20
1.5 Project Rationale	22
Chapter 2: Sexual Dimorphism in P0 DRG Cell Types Identified by Mass Cytometry	24
2.1 Abstract	24
2.2 Introduction	25
2.3 Materials and Methods	27
2.4 Results	33
2.5 Discussion	62
Chapter 3: Conclusions and Future Directions	67
3.1 Future Directions	67
3.1.1 <i>Examining Sexual Dimorphism</i>	67
3.1.2 <i>Mass Cytometry of Developing and Adult DRG</i>	69
3.1.3 <i>Further Examination of All Cell Populations in the DRG</i>	71
3.1.4 <i>Connecting Molecular Characterization with Cellular Function</i>	73
3.2 Conclusions	77
References	79

Acknowledgments

I would like to acknowledge the contributions provided by all of the faculty members involved with this project, Dr. Christopher Deppmann, Dr. Eli Zunder, Dr. Bettina Winckler, Dr. Hui Zong, Dr. Xiaowei Lu, Dr. Janet Cross, and Dr. Kevin Janes. I would also like to thank Dr. Robert Thorne for his support and encouragement. I have truly appreciated all of your time, feedback, support, and guidance as I worked toward completing this degree.

To Dr. Austin Keeler, I truly don't know what my PhD would have looked like without you. You're the kind of mentor who is willing to stand with me in front of the centrifuge to make sure I don't break it, even after you already carefully explained what went wrong the time I almost did break it. You taught me everything from mouse maintenance to cell culture to CyTOF data analysis, to what it means to be a great scientist and person. I am so grateful for your compassion, knowledge, friendship, and patience (which I know first-hand you have a lot of).

To my lab mates, you are all the best part of being in the lab. Science is hard and tough and wrought with failure, but having people on the ride with you makes it so much better. I'm so thankful for all the staff scientists, lab managers, postdocs, graduate students, and undergraduates I've gotten to work with over the last 5 years. You all have been so helpful and supportive of me, and so many of you are not just coworkers, but friends. Here are a few of the very many shoutouts I could give. Sushanth, I don't know how many questions I've asked you over the years, but you answered every one of them. You're the kind of lab mate who is willing to clean up the centrifuge after I almost broke it and not make me feel bad about it. Yu, thank you for making me laugh and always being willing to have ice cream with me. Brandon, thanks for being the kind of lab mate that I could have a chair race down the hallway with and for being one of my first friends in the lab. I also want to thank you for being such a brilliant scientist, but not making me, the fledgling baby grad student, ever feel bad about the many, likely uniformed,

questions I asked you. Ashley, you were my friend before you were ever my lab mate, but getting to have you be a part of both of those worlds has been such a treasure. I've always looked up to you as an incredible scientist, honest and caring person, and in so many other ways. If you've been this incredible of a scientist and person here, I can't wait to see you in full bloom. Katya and Sarah, you both are some of the most caring and compassionate people I have the privilege of calling my friends. I remember when you both joined the lab and how impressed I was with both of you and the talent, knowledge, and poise you displayed. I have no doubt, you both will go on to do the most magnificent things. To Paulina, Allison, Heeran, Hyebin, and August who I have had the privilege of working closely with and mentoring, I appreciate all of you and your hard work. I really would not have been able to accomplish what I have without the guidance, assistance, and support all of you have provided me. I only hope I provided some of the same things to you as well. To Najwa and Rusty, although I haven't known you both for long, I appreciate you taking me in as one of your own. From the first day I joined the Cloning Brigade, I was hit with some sarcasm, and I wouldn't have wanted it any other way. To all of the members of the Deppmann, Zunder, and Janes Labs, thank you for being some of the kindest and most supportive people I've had the privilege of meeting.

To my friends, especially my fellow graduate students in the 2017 cohort, you turned a brand-new city and state into a home. From basketball games, to peach picking, to board game nights. From ER visits, to finger surgeries, to hard days in the lab. From pumpkin picking, to hiking, to house parties featuring NyQuil. You all were there for the good, the bad, and the ugly. I wouldn't have wanted to go through this experience with anyone else.

To my family, thank you for the continued support throughout my life. Mom and dad, you have sacrificed so much for me and have truly been my biggest fans. I can't thank you enough for the lifetime of love, support, and encouragement you've given to me. Trey, we spent a lot of our

childhood bickering, but most of our adulthood, you've been helping me navigate the world. As you always used to say when we were kids, book smarts are not the same thing as street smarts. Although I think I'll always gravitate toward the side with books, I like to think I've learned a few things about practical intelligence from you. Thanks for being a supportive and protective big brother and someone I will always look up to. To all my in-laws, you have been some of the most welcoming, kind, and supportive people I've ever met. To Kelli, I've always wanted a sister and I am so lucky you got to be my first sister-in-law. I so appreciate the time we get to spend together, and I look forward to spending even more with you and baby Aria. To Heather, Heidi, Holly, Hannah, Hope, Helena, Ryan, Rodger, Hilary, Robert, and Haley and all of the spouses, although I gained a doozy of a last name, it was well worth it to be a part of such an amazing family. Tatiana, although we aren't related by blood, you truly feel like a sister to me. From being roomies our first year of grad school to being aged, married women out in the real world, I couldn't have asked for a better person to go through this, and all the other adventures (and misadventures) of life with.

To my husband, thank you. Richard, there are not enough words to express how grateful I am to have met and married you. As you well know, grad school is a rollercoaster, and although the ride has been going downhill for some time now, you have been by my side through all of it. You are the most selfless and supportive person and you've maintained that through every part of this journey. There are many people who helped make this dissertation theoretically possible, but you are solely responsible for helping to make it a reality. I can't thank you enough.

Abstract

Proper development of neuronal and glial populations in the dorsal root ganglia (DRG) is required for detection of touch, body position, temperature, and pain. While female-male differences in somatosensory perception have been previously reported, no study has examined global sex differences in the abundance of DRG cell types, and the developmental origin of these differences has not been characterized. To investigate whether sex-specific differences in neuronal and glial cell types arise in the DRG during development, we performed single-cell mass cytometry analysis on sex-separated DRGs from 4 separate litter replicates of postnatal day 0 (P0) mouse pups. In this analysis, we observed that females had a higher abundance of total neurons, as well as an increased abundance of TrkB⁺ and TrkC⁺ neurons responsible for mechanoreception and proprioception, respectively. Males had a higher abundance of TrkA⁺ neurons responsible for thermoreception and nociception. Pseudotime comparison of the female and male datasets indicates that male neurons are more mature and differentiated than female neurons at P0. These findings warrant further studies to better understand the origins and depth of sexual dimorphism in the DRG, develop protocols to conduct high dimensional proteomic analysis of adult DRG tissue, curate and develop more specialized antibody panels to better characterize distinct cell populations, and use additional tools to connect differences in molecular characterization to altered cellular function.

Chapter 1: Introduction to The Somatosensory Nervous System

The somatosensory nervous system revolves mostly around the sense of touch and responds to various tactile stimuli. The pathway from perception of a tactile stimulus to conscious recognition begins with first-order neurons in the periphery which synapse onto second-order neurons in the dorsal horn of the spinal cord. Second order neurons can then connect to third order neurons located in the brain, generally the brain region known as the thalamus^[1,2]. For the initial step of this pathway, first-order somatosensory neurons are located in either the trigeminal ganglia or the dorsal root ganglia (DRG). The trigeminal ganglia primarily houses first-order neurons that respond to stimulation of the face or head, while the DRG houses the first-order neurons that react to tactile stimulation for the rest of the body^[3].

Primarily focusing on the DRG, different populations of cells are responsible for detecting specific subtypes of tactile stimuli. These different cell types all originate from neural crest cells (NCCs), stem cells that differentiate into all of the cell types present in the DRG^[4]. A number of factors have been implicated in the migration of NCCs including cadherins, Noggin, and Rho-GTPases^[4-6]. The transcription factor Sox10 is pivotal for differentiation of NCCs into neurons, satellite glial cells, or Schwann cells. All NCCs express Sox10 initially, but neural progenitors will begin to lose Sox10 expression as development progresses, while glial progenitors will retain their Sox10 expression. As the glial cells continue to develop, Sox2 begins to be expressed in the Schwann cell, differentiating them from satellite glia^[7]. This introduction will further describe the neuronal and glial populations found in the DRG derived from these neural crest cells.

1.1 Somatosensory Neurons

Specific neuronal subpopulations are important for detection of itch (pruriception), pain (nociception), temperature (thermoception), touch (mechanoreception), and body positioning (proprioception)^[2,8-10]. The different classes of neurons responsible for the detection and response to each distinct stimuli diversify during development largely in part to neurotrophin expression in the surrounding environment^[11-13]. We will now review the functional and molecular characterization of these neuronal populations that has been well documented, primarily in adult mice, over the years.

1.1.1 Proprioceptors

Proprioception is the ability to detect one's body positioning in space and is related to balance. Three classes of neurons within the DRG known as 1a, II, and 1b muscle afferents are important for proprioception. Functionally, the main differences between these neuronal subtypes are where they innervate, project, and terminate. The 1a muscle afferents innervate muscle spindles. They project to the ventral spinal cord, and primarily terminate with direct connections to motor neurons^[14-16]. The 1b afferent neurons innervate the golgi tendon organs, serve as a point of connection for some interneurons involved with brain-ascending circuits, and terminate at the intermediate zone of the spinal cord. The II muscle afferents seem to resemble a mixture of the 1a and 1b afferent neurons, with a subset innervating, projecting, and terminating in regions similar to either the 1a or 1b muscle afferents^[2,8-10]. Molecularly, these specific neuronal populations originate from neural crest cells, as do all major neuronal subtypes in the DRG, and highly express neurogenin (Ngn) 1 and 2 during early development. Also observed in most neuronal populations in the DRG, distinct neuronal subgroups can be classified by expression of discrete tropomyosin-receptor kinases (TrkA, TrkB, or TrkC). Proprioceptors generally express high levels of TrkC in conjunction with Runx3^[2,8,10,17]. Although

three distinct populations of proprioceptive neurons have been discovered based on functional characteristics, the molecular profile within these three subtypes appears to be very similar according to scRNA-seq data^[2,8,10,17].

1.1.2 Low Threshold Mechanoreceptors

Mechanoreceptors respond to tactile stimuli and are involved with detection of innocuous as well as noxious touch^[2,8-10]. There are three subtypes of low threshold mechanoreceptors (LTMRs) responsible for mechanoreception in the DRG – A β -LTMRs, A δ -LTMRs, and C-LTMRs. Each mechanoreceptor subtype occupies distinct zones of the laminae in the spinal cord with some level of overlap. C-LTMRs which best detect light touch terminate in laminae II and are primarily identified by expression of tyrosine hydroxylase and vGlut3^[2,8-10]. A δ -LTMRs are capable of detecting dynamic movement and some degree of mechanical pain and terminate primarily in laminae III. Expression of TrkB until roughly weaning age, Piezo2, and NFH molecularly characterize this subpopulation^[2,8-10].

For A β -LTMRs, further characterization can be made between slowly adapting and rapidly adapting subtypes. Slowly vs rapidly adapting refers to how sustained the neuronal firing rate is after continued pressure is detected from a stimulus. Slowly adapting LTMRs show an increase in neuronal firing after application of a stimulus that is sustained throughout the duration of detection. In contrast, rapidly adapting LTMRs show increased firing after detection of a stimulus, which decreases or even ceases during the duration of stimulus application^[18,19,20,21,22]. All A β -LTMRs terminate in laminae III-V of the spinal cord and respond to some level of mechanical allodynia^[2,8-10]. The slowly adapting (SA) A β -LTMRs also respond to skin stretch or indentation and are molecularly characterized by their expression of NFH, Piezo2, and TrkC. The

rapidly adapting (RA) A β -LTMRs also respond to skin indentation along with deep pressure and can express NFH, Piezo2, and TrkB^[10].

1.1.3 Nociceptors

The last general neuronal population within the DRG are nociceptors. Nociceptors primarily respond to noxious stimuli and have subpopulations that encompass thermoreceptors and pruriceptors^[2,8-10]. There are 3 main subpopulations of nociceptors, however, these subpopulations can be further characterized as peptidergic versus non-peptidergic, which describes whether or not the neurons contain neuropeptides such as CGRP or Substance P^[2].

A δ nociceptors are lightly myelinated and terminate in laminae I and V of the spinal cord and are able to detect noxious stimuli like hair pull or pinpricks. Molecular characterization of this population is primarily identified by expression of TrkA, CGRP, Substance P, and peripherin, making all A δ nociceptors peptidergic. The other main population of nociceptors are C-fibers which are unmyelinated and can be further divided into peptidergic C-fibers and non-peptidergic C-fibers. Peptidergic C-fibers terminate in laminae I and primarily encompass thermoreceptors. They can be molecularly identified by expression of all of the same markers as the A δ nociceptors with the addition of TrpV1 and TrpM8 which sense hot and cold temperatures respectively. Non-peptidergic C-fibers terminate in laminae II of the spinal cord and can sense noxious pinprick along with pruriceptive subsets such as itch. Molecular identification of this nociceptor subpopulation is done through expression of IB4, PAP, MrgprA, and markers specific for particular chemical irritants such as MrgD4 for histamine and somatostatin for pruriceptors^[2,8-10].

Although neuronal populations receive the bulk of the attention when studying the somatosensory nervous system, other populations of cells can be just as important in the detection and response to peripheral stimuli. The most notable population of cells involved with detection and response to stimulation for the DRG are glial cells.

1.2 Glial Cell Development in the Periphery

In connection with the dorsal root ganglia, there are two main types of glial populations that support and modulate neuronal activity – Schwann cells (SCs) and satellite glial cells (SGCs).

1.2.1 Schwann Cells

SCs are primarily involved with the conduction of action potentials in the peripheral nervous system and can also provide trophic support to neurons and aid in repair after axonal injury^[23–25]. The SC lineage starts with migration of neural crest cells which encounter different regulatory factors that initiate gene expression changes which either promote or inhibit differentiation of neural crest cells into Schwann cell precursors, immature Schwann cells, and then more mature forms of SCs^[26]. Bone morphogenetic proteins (BMPs) and endothelins are some factors that inhibit differentiation of neural crest cells, while neuregulin-1 (NRG1), NOTCH, and fibroblast growth factor 2 (FGF2) promote differentiation. Some of the transcriptional regulators that have been heavily implicated in the development of Schwann cells include SOX10 and EGR2 (also known as KROX20). EGR2 is a zinc finger transcription factor that is highly involved with maintaining and ending SC differentiation. Sox10 is a transcription factor involved in many processes during early development. It is first expressed before neural crest cell migration and is required for initial differentiation of neural crest cells and further differentiation of SCs^[26,27,28].

Mature SCs can be divided into myelinating and non-myelinating (Remak) subpopulations. Non-myelinating SCs, also known as Remak bundles, are normally associated with small diameter neurons in the DRG. Myelinating SCs tend to associate with larger diameter neurons and are important for impacting the conduction speed of action potentials^[29]. Multiple studies have shown whether or not an axon is myelinated can impact how that neuronal subtype responds to different stimuli^[18,20,21].

The determination of which axons are myelinated or not is dependent, in part, on axonal diameter, however, association of myelinating SCs with specific axons can also be controlled by specific molecules or factors. Studies have shown that laminin receptors, specifically through proper function of $\beta 1$ integrin, are important for proper association of Schwann cells with neurons^[30]. Similarly, cell adhesion molecules, including neural cell adhesion molecule (NCAM), have also been shown to play a role in proper association and myelination of axons^[31]. Additionally, one previous study has shown that NGF, the ligand for TrkA, can promote myelination by Schwann cells but not oligodendrocytes^[32]. Taken together, these studies show that axonal diameter, expression or downregulation of different molecules, and activation of TrkA on peripheral axons can all impact myelination in the DRG^[23].

1.2.2 Satellite Glial Cells

In addition to Schwann cells, satellite glial cells (SGCs) also develop in the periphery and play a role in support and modulation of neurons in the DRG.

SGCs also develop from neural crest cells and are known to surround the cell bodies of peripheral neurons^[33]. One key function of SGCs is to promote homeostasis of the environment

around these neurons. Autoradiographic studies have demonstrated this by showing that SGCs can uptake GABA and glutamate^[34,35] and also express potassium channels^[36,37]. As depolarized neurons release potassium, SGCs play an important role in taking up excess potassium and thus maintaining the extracellular environment around neurons^[38,39]. In addition to modulating ions and neurotransmitter levels, SGCs also help create an ideal environment for neurons by acting as phagocytes for debris during early development^[40]. During peripheral nervous system development, there is an overproduction of neurons that eventually undergo a large apoptotic event in which approximately 50% of the neurons are eliminated^[41,42]. This process of culling excess neurons begins around embryonic day 11 and is mostly concluded by embryonic day 15, generally before macrophages have infiltrated into the periphery^[40,43]. During this time period before the presence of macrophages, SGCs are able to phagocytose the neuronal debris in the extracellular environment, thus improving the growth and survival of the remaining, healthy neurons^[40,33,44].

Molecularly, expression of TrkB, BFABP, glutamine synthase (GS), and the protein S100 are all markers used to identify SGCs^[45-47]. Some of the markers and genes used to identify SGCs, in particular S100, overlap in expression with SCs. This makes localization of expression vital for informing which cell type is being observed^[33,47-50].

Overall, the three broad cell populations present within the DRG (neurons, Schwann cells, and satellite glial cells) all emerge from neural crest cells in the early embryonic stages of development and go through various morphological, molecular, and functional changes by the time the mouse pup is born (Figure 1).

Figure 1:

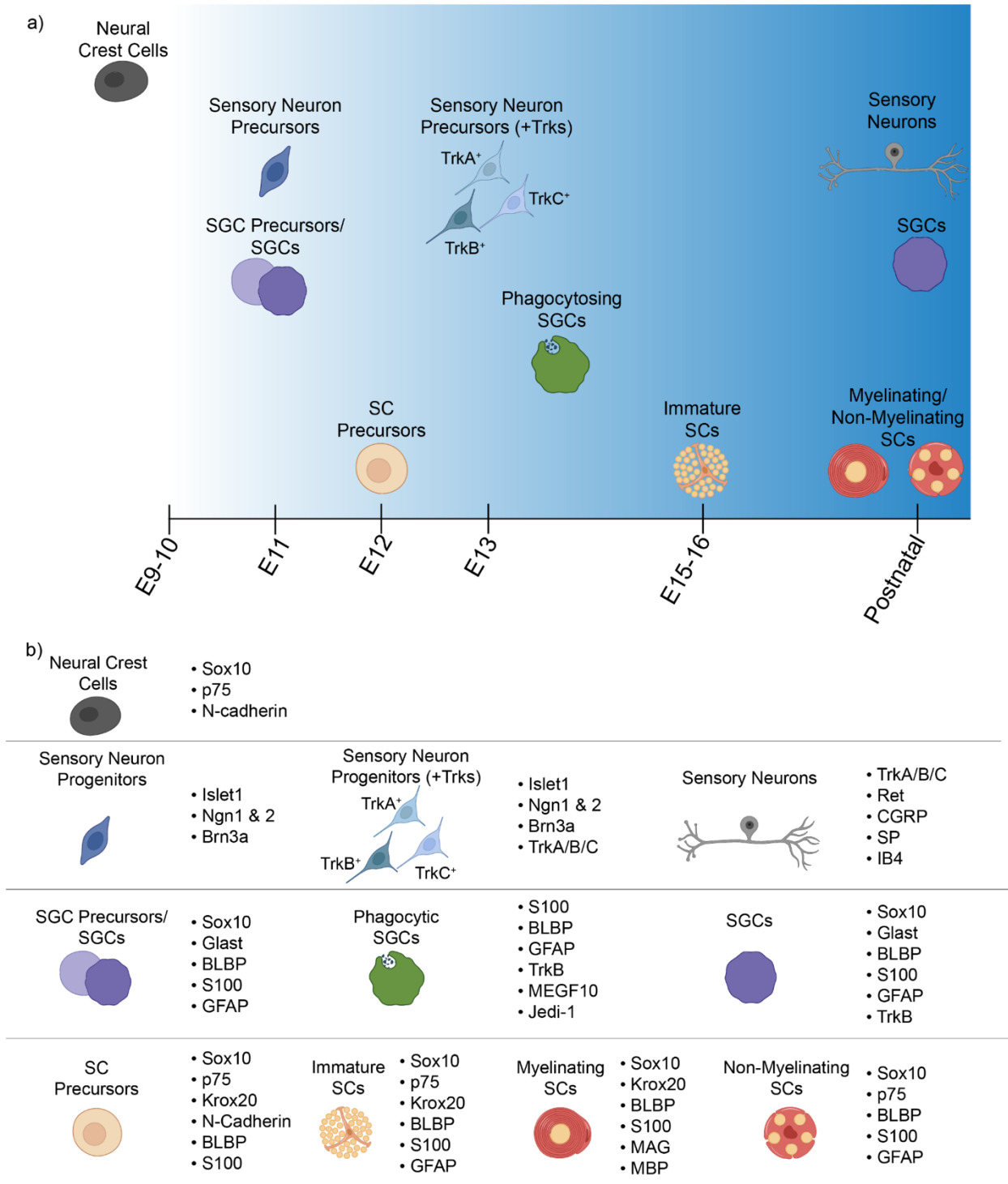


Figure 1: Schematic depicting developmental timeline for peripheral neuronal and glial populations with key markers expressed for each population. a) Timeline depicting the

general developmental period when neuronal or glial populations emerge. Most peripheral cells are derived from neural crest cells. Around E11, satellite glial cell (SGC) precursors/SGCs and sensory neuron progenitors begin to develop. Schwann cell (SC) precursors begin to emerge around E12. Around E13, sensory neurons begin to express Trk receptors that help guide them to their final targets in which competition for limiting growth factors ensues, leading to the death of about half of the original sensory neuron progenitor pool. About a day after this large apoptotic event is occurring, some of the SGCs will phagocytose the resulting debris. Around E15, the SC precursors will differentiate into immature SCs. By birth, many mature sensory neuron populations have formed and associated with mature SGCs. Additionally, SCs will have further differentiated into myelinating and non-myelinating SCs. b) Key markers used to identify developing neurons and glia.

1.3 Single-Cell Analysis in the DRG

Although the broad characterization of the different neuronal and glial populations has been well documented on a macro level, studies utilizing single cell analysis have started emerging to better categorize the specific and distinct differences within and between cell types in the DRG.

Before the development of single-cell analysis tools such as single-cell RNA-sequencing (scRNA-seq), techniques like microarrays were commonly used to assess gene expression. Microarrays were a powerful tool for better understanding and identifying gene expression^[51,52]. Although initially this technique was limited in that cells could only be assessed as a group and not individually, advances in the field made it possible to also use microarrays to examine single cells^[53,54]. Regardless of whether or not an individual or group of cells were examined, one major limitation of microarrays remained – only known genes could be assessed with this technique. RNA sequencing helped address these limitations by directly sequencing the RNA,

thus allowing for a practically unlimited amount of RNA expression information to be acquired^[55]. Ultimately, this direct RNA sequencing technique was adapted for single-cells and multiplexed to allow for even higher throughput analysis of RNA within individual cells, allowing for much more comprehensive and thorough analyses of distinct cell populations within a wide variety of tissues^[56,57].

Many bulk and single-cell RNA sequencing studies have been published better characterizing the neuronal and glial populations found specifically within the DRG. For neurons, multiple papers have used RNA sequencing to better identify distinct neuronal subtypes, examine differences in gene expression between DRG neurons from different regions of the spinal column, and used RNA sequencing with time course studies to examine neuronal development from embryonic timepoints through adulthood^[17,58–60]. Similarly, diversity in peripheral glial populations has also been examined with this technique^[50,61]. Although all of these studies have helped better molecularly characterize the neuronal and glial cell populations within the DRG, there are still gaps in knowledge created by using this technique.

Two main shortcomings of RNA sequencing are (1) the number of cells able to be analyzed at once and (2) the reality that the amount of RNA transcript does not always equal the amount of protein. Although the ability to survey an unlimited number of genes is incredibly valuable, especially when little is known about the expression profile of the population of cells being examined, this limits the number of cells that can be analyzed at one time. Although this likely won't be much of an issue for highly abundant cell populations, it can result in rare cell populations being excluded from study. Additionally, the ability to examine RNA can be very useful for implying what likely proteins will be transcribed and thus what functionality is likely for the observed cell. However, the ratio of RNA transcript to protein is rarely 1:1. RNA could be degraded before translation, or not translated at all. This means that although RNA sequencing

may be able to highlight the RNA expression for a variety of different genes, there is no guarantee those genes will be transcribed into protein and thus produce the expected function^[62–68]. Conversely, the RNA could be transcribed into protein, but the protein could be degraded, resulting in a skewed ratio of RNA to protein^[69]. Because of these limitations with RNA investigation, it is important to also assess protein expression when aiming to molecularly characterize distinct cell populations.

One technique that allows for the assessment of protein in single cells is FLOW cytometry. The instrumentation behind the flow cytometry machine or fluorescence activated cell sorter (FACS) instrument was developed in the early 1970s^[70]. The general methodology of FLOW cytometry is that the instrument is able to create single-cell droplets that can either be counted, sorted, or measured based on a specific criteria such as fluorescence^[70,71]. The ability to label specific proteins with fluorescent markers and then assess a large number of cells individually for their expression of those proteins is incredibly valuable. For some scientific questions, the ability to look at a few different proteins is sufficient, thus making FLOW cytometry a valuable tool. However, for scientific studies that wish to assess more than a few proteins at a time, the spectral overlap between fluorescent markers greatly limits the number of proteins that can be assessed at one time.

The benefit of RNA sequencing's ability to examine thousands of RNA transcripts has the caveat of only being able to examine a limited number of cells with no ability to determine if the detected RNA expression will be translated into protein. For FLOW cytometry, the ability to inspect protein expression specifically within a larger number of cells is incredibly valuable, but the spectral overlap between fluorescent markers restricts the number of proteins that can be examined within any individual cell. A more recent technique that is able to address some of the drawbacks of RNA sequencing and FLOW cytometry is mass cytometry.

Mass cytometry is a variant of flow cytometry that uses antibodies and other affinity reagents labeled with isotopically pure rare earth metals to quantify biomolecule abundances in single cells by atomic mass spectrometry. As there is very little spectral overlap between rare earth metal isotopes, this approach enables simultaneous measurements of over 40 molecular markers per cell^[72]. Although mass cytometry is most commonly used to quantify immune cell types in the blood and other tissues, our lab was able to adapt this technique for neural tissues^[45,73] (Figure 2). In our recent publication, we were interested in doing a more thorough protein-level analysis of neuronal and glial development within the DRG by examining the expression levels of approximately 40 different markers every day from embryonic day 11.5 to postnatal day 4. The resulting analysis of roughly 2.8 million cells highlighted the power of mass cytometry for examining expression of a larger number of proteins within single cells. Our study also found that this technique for protein-level analysis was able to identify most of the neuronal populations identified by RNA sequencing, but was additionally able to uncover more rare populations that are likely harder to detect with RNA sequencing^[45].

Figure 2:

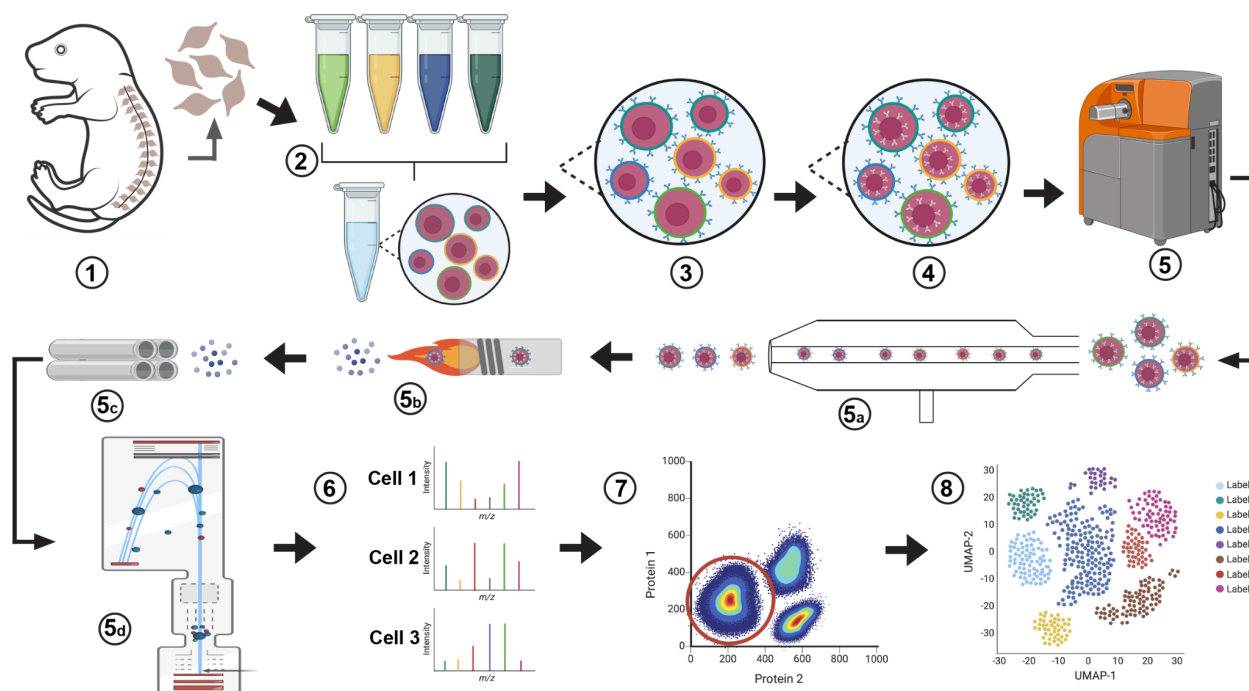


Figure 2: Schematic depicting process for collecting, preparing, and examining neural samples with mass cytometry. 1) DRGs are dissected from the spinal column of a mouse pup. 2) The DRGs collected are dissociated into single-cells. This process is repeated for all samples. Each sample is then barcoded and pooled. 3) The pooled and barcoded cells are then stained for extracellular epitopes with metal label antibodies. 4) Following extracellular staining, the cells are methanol permeabilized and stained for intracellular epitopes with metal labeled antibodies. 5) The samples are then run through the Helios CyTOF 2 single-cell mass cytometer. 5a) The mass cytometer works by nebulizing the cell mixture into single cell droplets. 5b) These droplets then travel through an inductively coupled argon plasma (ICP) flame which incinerates the cells, but not the metal ions, thus resulting in an ion cloud. 5c) The ion cloud travels through a quadrupole to enrich the heavy metal ions. 5d) The heavy metal ion cloud is then quantified by time-of-flight mass spectrometry for each cell. 6) The metal ion signal intensity is quantified for each cell and converted into an FCS file. 7) The FCS file can then be normalized and debarcoded and used in conjunction with websites like Community CytoBank to

gate out debris or multiple cell aggregates. **8)** Once the data has been cleaned, it can be further analyzed, typically with some type of clustering algorithm and dimensionality reduction software to produce images like this example UMAP. This allows us to easily visualize differences in expression of the antibodies used in our panel which can inform us about different cell populations or cell states.

Taken together, previous studies have been instrumental in functionally and molecularly characterizing the neuronal and glial populations within the DRG generally throughout development. With the advent of single-cell analysis techniques like RNA sequencing and mass cytometry, even more thorough characterization of distinct cell populations and subpopulations is possible.

1.4 Molecular and Functional Sexual Dimorphism in Somatosensory Cell Populations

In the nervous system broadly, studies have been conducted that highlight the role of sex in nervous system development and disease. Specifically, the steroid hormone estradiol has been implicated in driving sex differences observed in nervous system development. Numerous studies have shown the impact of estradiol in promoting sex differences in cell differentiation and proliferation^[74–77], neurite outgrowth^[78,79–81, 82,74–77], synaptic patterning^[83,77,84–86], cell number and apoptosis, thus affecting volumetric size^[77,87–94], and sexual and social behaviors^[77,95–100].

Although some studies have been conducted highlighting the role of estradiol in peripheral nervous system development and function^[101–103], most of this research has been concentrated in the central nervous system. Similarly, most studies examining molecular characterization of cell types in the DRG lack much description of the role that sex may play in the expression of specific genes or proteins. Recently, many studies have been published highlighting the

disparities that exist between biologically female and male human patients in some pain disorders and potency of response to analgesics^[104–109]. Utilizing mouse and rat models have provided some insight into potential sources of the sexual dimorphism displayed in pain sensation and analgesic response.

A few studies have shown functional sex differences in baseline pain levels. One paper showed sex differences between male and female pups in hot plate and tail withdrawal latencies at postnatal day 0 (P0) and P7. Particularly for the hot plate, males had an increased latency to paw withdrawal when compared with females^[110]. Another publication investigated sexual dimorphism in response to thermal pain over the course of development. They found that significant sex differences were detected by P12 and persisted into adulthood for their particular test. Similarly, males had an increased latency to response when compared to females^[111]. In addition to analysis of functional differences in analgesic response between sexes, many studies have also started characterizing molecular sex differences between the neuronal populations underlying these functional responses. One study found multiple differentially expressed genes between males and females when examining neurons from different regions of the spinal cord in embryonic day 18.5 (E18.5) pups, adult mice, and in an enriched population of TrpV1⁺ neurons^[59]. An additional study using RNAseq found differentially expressed genes from DRG neurons in which female neurons seemed to have an upregulation in genes responsible for regulating immune processes, growth factors, synaptic proteins, and channels, while males showed upregulation of genes that modulate anabolism, oxidative phosphorylation, and antioxidant pathways^[112]. Taken together, these studies show under normal conditions what sexual dimorphism exists in analgesic response as well as in the gene expression of neurons. One limitation of the molecular characterization of sex differences in neurons is that no single-cell, high-throughput analysis has been performed to date to examine this question under standard conditions.

While not completed under standard conditions, single-cell, high-throughput analyses, along with functional examination, has been conducted on neuronal and glial cells in the periphery after perturbing the system through injury or increased inflammation^[113–119]. Although gaining a better understanding of sex differences in neuronal response or molecular composition is invaluable for the eventual treatment of injury or inflammation-induced disorders, there is still a gap in the molecular characterization of neuronal and glial populations at the single-cell level in a high throughput manner.

1.5 Project Rationale

There has been a large effort over the past few decades to provide a more comprehensive functional and molecular characterization of neuronal and glial cells in the DRG. This has been accomplished with multiple behavioral studies as well as bulk and single-cell RNA and protein analyses on different cell populations. Simultaneously, the scientific community has been enlightened about the importance of examining differences between sexes not only in the response to painful stimuli or analgesics, but also in the expression of molecular markers that help identify different cell types as well as impact their functionality. Although some studies have started to undertake the task of examining sexual dimorphism in the DRG, no study to date has harnessed the power of single-cell techniques to examine sexual dimorphism under standard conditions. For my project, I aim to address this gap in knowledge by using single-cell protein-level analysis to determine if sex differences exist in the abundance of different neuronal and glial populations at postnatal day 0. This work highlights the power of being able to examine roughly 40 different protein markers within single-cells in a robust manner to identify large and subtle sexual dimorphism between specific populations and sub-populations of neurons and glial in the DRG. This project has the potential to offer another approach for analyzing single-cell

data and provide additional rationale for the importance of continuing this work of examining sexual dimorphism at a single-cell level across different tissues and timepoints.

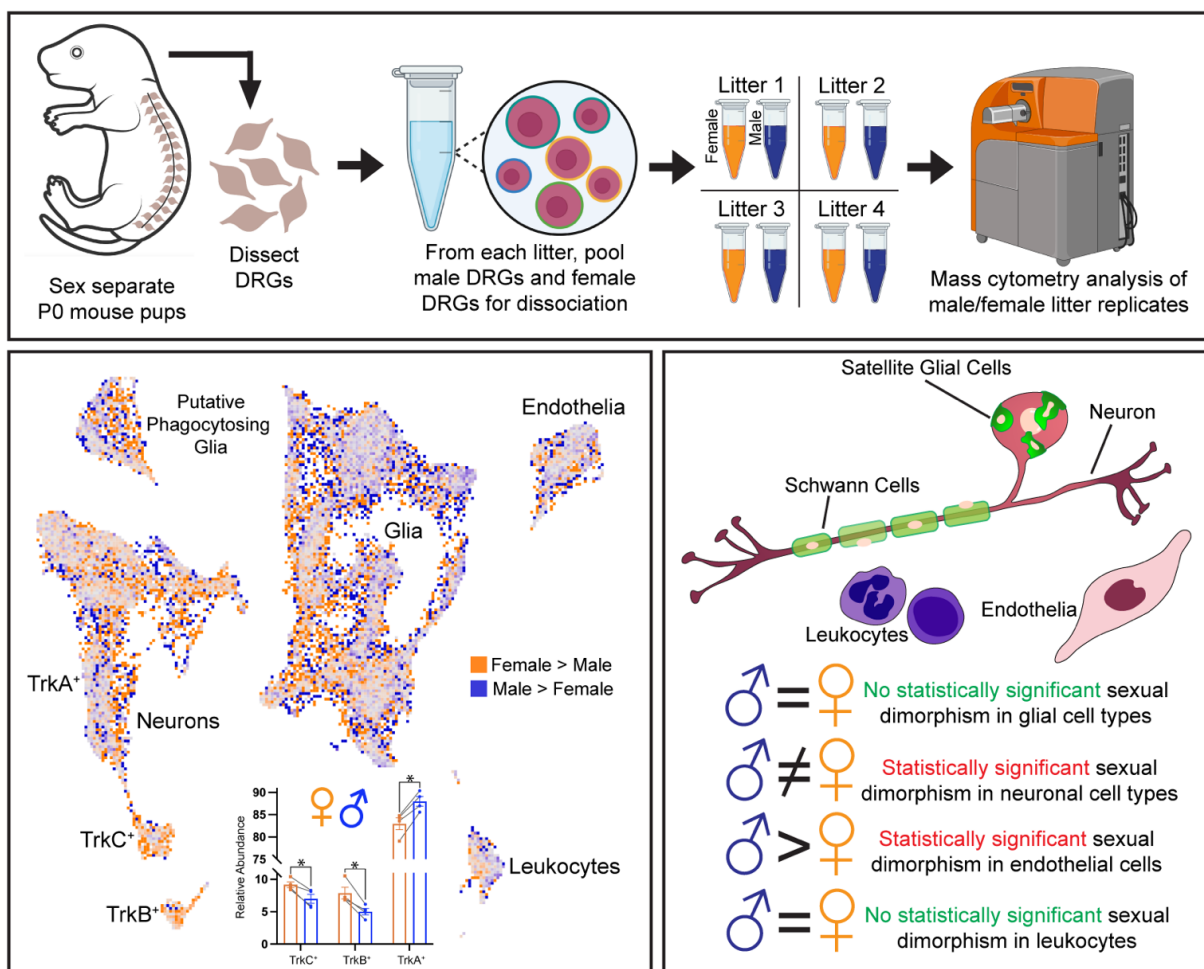
Chapter 2: Sexual Dimorphism in P0 DRG Cell Types Identified by Mass Cytometry

2.1 Abstract

Development of neuronal and glial populations in the dorsal root ganglia (DRG) is required for detection of touch, body position, temperature, and noxious stimuli. While female-male differences in somatosensory perception have been previously reported, no study has examined global sex differences in the abundance of DRG cell types, and the developmental origin of these differences has not been characterized. To investigate whether sex-specific differences in neuronal and glial cell types arise in the DRG during development, we performed single-cell mass cytometry analysis on sex-separated DRGs from 4 separate litter replicates of postnatal day 0 (P0) C57/BL6 mouse pups. In this analysis, we observed that females had a higher abundance of total neurons ($p=0.0266$), as well as an increased abundance of TrkB⁺ ($p=0.031$) and TrkC⁺ ($p=0.04$) neurons for mechanoreception and proprioception, while males had a higher abundance of TrkA⁺ ($p=0.025$) neurons for thermoreception and nociception. Pseudotime comparison of the female and male datasets indicates that male neurons are more mature and differentiated than female neurons at P0. These findings warrant further studies to determine whether these differences are maintained across development, and their impact on somatosensory perception.

Keywords: sexual dimorphism, somatosensory neurons, mass cytometry, dorsal root ganglia

Graphical Abstract



2.2 Introduction

First-order somatosensory neurons in the dorsal root ganglia (DRG) innervate skin, muscle, and other tissues of the body to detect percepts such as pain, temperature, touch, and body position^[1]. In addition to the neuronal populations, Schwann cells and satellite glial cells (SGCs) in the DRG also play a role in somatosensory perception. Schwann cells play an important role in myelination, which increases action potential conduction velocity^[120], and SGCs have been implicated in the regulation of pain response, formation of synaptic structure, and modulation of neuronal survival and activity in the periphery^[49,121,122]. Molecular characterization of neuronal

and glial populations in the DRG will improve our understanding of how these cells develop and mature to generate a functional somatosensory nervous system, as well as provide insights into potential therapeutics for somatosensory disorders such as chronic pain or peripheral neuropathy.

Decades of work utilizing immunofluorescence, genetic manipulation, and electrophysiology have delineated distinct neuronal and glial cell types in the mouse DRG^[2]. More recently, single-cell measurements by scRNA-seq^[2,17,60,61] and mass cytometry^[45] have improved the molecular resolution for these cell types. With thousands of transcripts measured per cell, scRNA-seq is well-suited for unbiased screening and discovery, while the higher throughput and protein-level readout of mass cytometry make this technique well-suited for replicate comparisons of cell types defined by their functional biomolecules.

Mass cytometry is a variant of flow cytometry that uses antibodies and other affinity reagents labeled with isotopically pure rare earth metals to quantify biomolecule abundances in single cells by atomic mass spectrometry^[72]. Using commercially available rare earth metal isotopes, this approach enables simultaneous measurements of over 40 molecular markers per cell. Although mass cytometry is most commonly used to quantify immune cell types in the blood and other tissues^[73], we recently adapted this technique for neural tissues and used this approach to profile nearly 3 million neuronal and glial cells from the mouse DRG across 13 days of embryonic and postnatal development^[45]. Mass cytometry and scRNA-seq have provided a detailed molecular characterization of cell development in the DRG, but one question remains unaddressed: is DRG development sexually dimorphic? Sex differences in response to pain and other somatosensory stimuli^[119] as well as sexual dimorphism in the efficacy of analgesics in humans have been previously observed^[114,123]. We hypothesized that these differences could be due to differences in DRG cell type abundances or expression profiles between females and

males that could begin during development and persist into adulthood. Therefore, analysis of sexual dimorphism in development could serve as the initial step toward better understanding the underpinnings of sex differences observed in adults.

Previous studies have identified sexually dimorphic patterns of RNA expression in the DRG by bulk RNA-seq^[59,112], but no single-cell comparison has been performed to determine which (if any) somatosensory cell types differ in abundance between females and males. To address this gap in knowledge, we used our previously validated neural mass cytometry platform^[45] to profile female and male DRG litter replicates at P0 for statistical comparison. In this analysis, we observed that females have a larger relative abundance of neurons overall, especially within TrkB⁺ and TrkC⁺ subtypes, while males have a larger relative abundance of TrkA⁺ neurons. Further examination of markers, such as MAP2, and utilization of pseudotime analysis revealed that neuronal populations in females appeared less mature when compared to males. These findings demonstrate a clear dimorphism between females and males, particularly in neuronal populations, and represent a promising area for future study across embryonic development, postnatal development, and into adulthood.

2.3 Materials and Methods

Animals

All animal experiments were carried out in compliance with policies of the Association for Assessment of Laboratory Animal Care and were approved by the University of Virginia Animal Care and Use Committee (Deppmann protocol no. 3795). Pregnant C57BL/6J female mice were ordered from Jackson Labs and tissue was collected from sex-separated postnatal day 0 pups. Pups were sexed as previously described by examining differences in anogenital pigmentation: male pups have a pigmented spot that eventually develops into the scrotum, while female pups do not^[124]. Animals were housed on a 12-hour light/dark cycle with food and water ad libitum.

Sample Collection and Processing for Mass Cytometry

DRG dissection, dissociation, fixation, and staining were performed as previously described^[45]. DRG were plucked from the vertebrae, combined from all four regions of the spine, and pooled by sex for each litter. Following removal, DRGs were incubated in Enzyme Solution 1 (5mg ml⁻¹ BSA, 2 mg ml⁻¹ Collagenase Type 2, 0.2 mg ml⁻¹ DNase-I, and 0.2 mg ml⁻¹ hyaluronidase in DMEM/F-12) for 20 minutes and Enzyme Solution 2 (1.5 mg/ml trypsin in DMEM/F-12) for 15 minutes. Three fire-polished pipettes with decreasing pore diameter were used to mechanically dissociate the tissue into a single-cell suspension. Cells were then incubated in 10µM cisplatin in PBS as a cell viability dye for 30 seconds before quenching with PBS containing 0.5% BSA. Cellular responses to cisplatin, such as DNA damage, occur on a longer time scale (hours) than the one used in this study^[144-145]. Cells were centrifuged at 300 x g for 3 minutes at 4°C and washed with the quenching solution before fixation in 1mL of 1.6% PFA solution in PBS for 10 minutes at room temperature. Following fixation, cells were washed in PBS before final resuspension in cell staining medium (CSM; 0.5% BSA and 0.02% NaN₃ in PBS). Separate 1.5mL microtubes and pipettes were used for samples from different sexes. Samples were stored at -80°C after fixation until collection was complete for all four litters.

Mass Cytometry

To improve sample uniformity, individual samples were Palladium barcoded and then pooled for antibody staining and mass cytometry measurement^[125,126]. Surface and intracellular antibodies used in this study are listed in Figure 4, along with the total number of animals included in each sample, and the number of cells analyzed in each sample. Cells were analyzed on a Helios CyTOF 2 System (Fluidigm Corporation) by the University of Virginia Flow Cytometry Core (RRID: SCR_017829) at the rate of 200-300 cells/second.

Post-Run Sample Processing

All .FCS files from the mass cytometry run were bead normalized^[127] and debarcoded as previously described^[125,126]. To isolate single cells from fragments/debris and cell aggregates, clean-up gating was performed with Cytobank (<https://community.cytobank.org/cytobank/>) (Figure 5).

High Dimensional Analysis

Analysis was performed as previously described^[45]. Briefly, cells were partitioned with Leiden clustering (<https://github.com/vtraag/leidenalg>)^[128] to identify molecularly defined cell types, with the nearest neighbors parameter set to 15. To assess if clusters were homogenous and unimodal, we inspected violin plots of marker expression for each cluster. To improve the molecular resolution of cell populations, cell types of interest were subjected to multiple rounds of Leiden clustering. For the first round of clustering (primary clustering) and all subsequent rounds of clustering (secondary and tertiary), all 40 expression markers were used. Cluster identity was manually annotated by examination of marker expression and comparison with previously reported expression profiles of distinct DRG cell types. 40-dimensional mass cytometry datasets (including all antibody markers) were embedded into 2 dimensions by uniform manifold approximation and projection (UMAP)^[129,130] (release 0.2.4, <https://github.com/lmcinnes/umap/releases/tag/0.2.4>) with the following parameters: nearest neighbors = 15 (except for the secondary clustering of neurons which had a nearest neighbors = 50), metric = Euclidean, local connectivity = 1, components = 2, epochs = 1000^[45,130]. The software code used for Leiden clustering and UMAP embedding is provided with this manuscript, as described below in the section Code Availability.

Abundance Comparison UMAP

To visually inspect differences in cell type abundance between female and male samples across all cell types and molecular phenotypes, we plotted the log₂-fold ratio at every location on a 2D UMAP layout. To make this calculation, the UMAP plot was divided into two-dimensional bins corresponding to pixels on the plot, and then number of female vs. male cells within each bin was used to calculate the log₂-fold ratio. These bins are defined by regular intervals along the x and y axes, which serve as the boundaries for the quantitative relative abundance analysis conducted within each pixel. As some bins only contained all female or all male cells, we manually set the value for these as 10% greater than the absolute maximum observed female/male ratio. Further details and code to run this abundance comparison analysis are available at <https://github.com/zunderlab/Vradenburgh-et-al-P0-DRG-Sexual-Dimorphism-Manuscript>.

Multi-Trk⁺ Quantification

To identify multi-Trk⁺ neuronal populations based on expression of the three Trk receptors, we calculated the 1st-15th percentile expression levels for each Trk in a cluster known to highly express one of each three Trk receptors. Positivity was determined based on cluster assignments for secondary clustering of only neuronal populations with TrkA positivity determined by 2-Non-Pep, TrkB positivity by TrkB⁺ neurons, and TrkC positivity by TrkC⁺ neurons. These values were used as thresholds to identify positive expression for each Trk receptor. Cells that expressed pairs of Trk receptors above this threshold were classified as multi-Trk expressing.

Developmental Cell Trajectories with URD

Code for the URD algorithm (<https://github.com/farrellja/URD>)^[131] was modified for compatibility with mass cytometry. URD analysis conducts random walk iterations for every cell from a manually selected “root” to manually selected “tips”. URD then assigns each cell a pseudotime

value that relates to its developmental trajectory as opposed to actual age. We proportionally downsampled our data only for this analysis so each sample consisted of the same number of cells.

Tissue Processing for IHC

One female and one male pup from 6 separate litters were euthanized by decapitation. The lower lumbar spinal columns were dissected and fixed in 4% PFA overnight before cyroprotection in 30% sucrose in PBS for 2 days, all at 4°C. The tissue was subsequently embedded in OCT (VWR, 25608-930) and then cryosectioned into 30- μ m sections and stored at -80°C. The L4/5 DRG were analyzed using the last rib as a landmark for T13.

Immunostaining

Mounted sections were warmed to room temperature and washed with PBS three times for 5 minutes each. Antigen retrieval was performed for all antibodies by microwave boiling slides/sections in sodium citrate buffer (10 mM sodium citrate, pH 6.0). Sections were cooled to room temperature; sodium citrate buffer was replaced; and sections were microwaved until boiling again. Sections were then rinsed three times with PBS and incubated with blocking solution (0.1% Triton X-100 and 3% normal donkey serum) for 1 hour at room temperature. Sections were incubated with primary antibodies diluted as detailed below in blocking solution overnight at 4 °C. Sections were washed with PBS three times for 5 minutes each, incubated with secondary antibodies for 1 hour at room temperature protected from light and then washed with PBS four times for 5 minutes each. Sections were mounted in Fluoromount-G with DAPI (SouthernBiotech). Primary antibodies used in this study: rabbit anti-Islet1/2 (Abcam, ab275990, 1:100, RRID: AB_10866454), rabbit anti-TrkA (Millipore Sigma, 06-574, 1:100, RRID: AB_310180), and goat anti-TrkC (R&D Systems, AF1404, 1:1,000, RRID: AB_2155412). Secondary antibodies used in this study: Alexa Fluor 488 donkey anti-rabbit (Thermo Fisher

Scientific, A-21206, 1:500, RRID: AB_2535792) and Alexa Fluor 647 donkey anti-goat (Thermo Fisher Scientific, A-21447, 1:500, RRID: AB_2535864).

Cell Count Quantification

A blinding protocol preceded the imaging of all tissue was imaged on the laser scanning confocal Zeiss 980 NLO at $\times 20$ or $\times 40$ resolution in Z-stacks at 0.5- μm intervals. All images were taken with the same exposure time for each channel and manually analyzed using Fiji software for the presence or absence of fluorescence corresponding to expression of Islet1, TrkA, or TrkC. Cells expressing Islet1, TrkA, or TrkC were counted and compared to counts of all cells determined from counting DAPI-stained nuclei. In total, 11,718 DAPI⁺ cells from female pups and 8,646 DAPI⁺ cells from male pups were examined for Islet1 analysis (Figure 6m-n) and a total of 1,401 Trk⁺ neurons from female pups and 2,327 Trk⁺ neurons from male pups were examined for the TrkA and TrkC analysis (Figure 11e-f).

Data/Code Availability

Access to the FCS files before normalization or debarcoding is available on Flow Repository at <http://flowrepository.org/id/FR-FCM-Z687>. Access to the gated files is available on Community Cytobank at <https://community.cytobank.org/cytobank/experiments/110082>. All code used to perform the analysis described in this manuscript is available on GitHub at <https://github.com/zunderlab/Vradenburgh-et-al-P0-DRG-Sexual-Dimorphism-Manuscript>.

Experimental Design and Statistical Analyses

For mass cytometry experiments, P0 mouse pups were collected from 4 separate litters and separated into two groups by sex. The number of pups per litter varied from 6 to 8, and these numbers are reported in Figure 4. DRGs were dissected from sex-separated pups from each litter and pooled into sex-separated tubes, and the male and female pooled samples were

processed separately for mass cytometry as described above. Once DRGs were collected and stored from all replicate litters, they were thawed and barcoded for mass cytometry analysis. After data preprocessing, there were 32,461 female cells and 28,161 male cells. For comparative analyses of cell type abundances, percentages are reported as a relative percent for each individual sex-separated sample.

Statistical Analysis

Examination of sex differences in relative cell type abundance were analyzed using multiple unpaired t-tests on GraphPad Prism 9.3.1. The results of statistical tests performed are detailed in the text and figure legends as well as Figure 10, Figure 13, Figure 15, Figure 17. $p < 0.05$ was considered statistically significant and the exact p value is reported for each comparison either in the figure or associated supplementary data figure.

2.4 Results

Characterization of Sex-separated Cell Populations in the Developing DRG by Mass Cytometry

To investigate whether somatosensory cell types are sexually dimorphic in the developing DRG, P0 mouse pups were separated by sex from individual litters, and the male and female DRGs were pooled separately for single-cell dissociation and PFA fixation. This same sample collection was performed on 4 litter replicates, resulting in 8 samples total that were stored at -80°C before being thawed, barcoded, stained with metal-conjugated antibodies, and then analyzed on a CyTOF Helios mass cytometer instrument (see methods, Fig. 3a). To identify all cell populations in the DRG (e.g., neurons, glia, endothelia, macrophages, leukocytes), the antibody panel from our previous DRG study^[45] was applied with minor modifications (Fig. 4). After data pre-processing and clean-up gating (Fig. 5), female and male samples were pooled

for Leiden clustering (60,622 cells) to separate all cells into distinct groups based on their molecular profile and plotted in 2 dimensions by UMAP (Fig. 3b). Distinct cell types and populations were identified by comparing the protein expression profile of each cluster with known cell type markers[45] (Fig. 3c). This approach separated TrkA⁺, TrkB⁺, and TrkC⁺ neurons, putative phagocytosing glia, immature glia (Im. glia), satellite glial cells (SGCs), Schwann cells, endothelial cells, macrophages, and leukocytes (specific markers used for identification can be found in Fig. 4). Cells with no markers expressed or very few markers at low levels were categorized as low complexity or unidentified. These cells comprise 2.2% of all DRG cells measured and were not included in the calculations of relative abundance for additional rounds of clustering presented in Figures 6,8,9,11,12,14,16, and18. To investigate variability in cell type abundance between litters, the standard error of the mean (SEM) was compared for each cell type (Fig. 3d). Endothelial cells, leukocytes, and macrophages have the lowest SEM values (below 0.3), while glial and neuronal cells have a wider range of SEM values spanning 0.2 to 1 between individual litter samples.

Figure 3

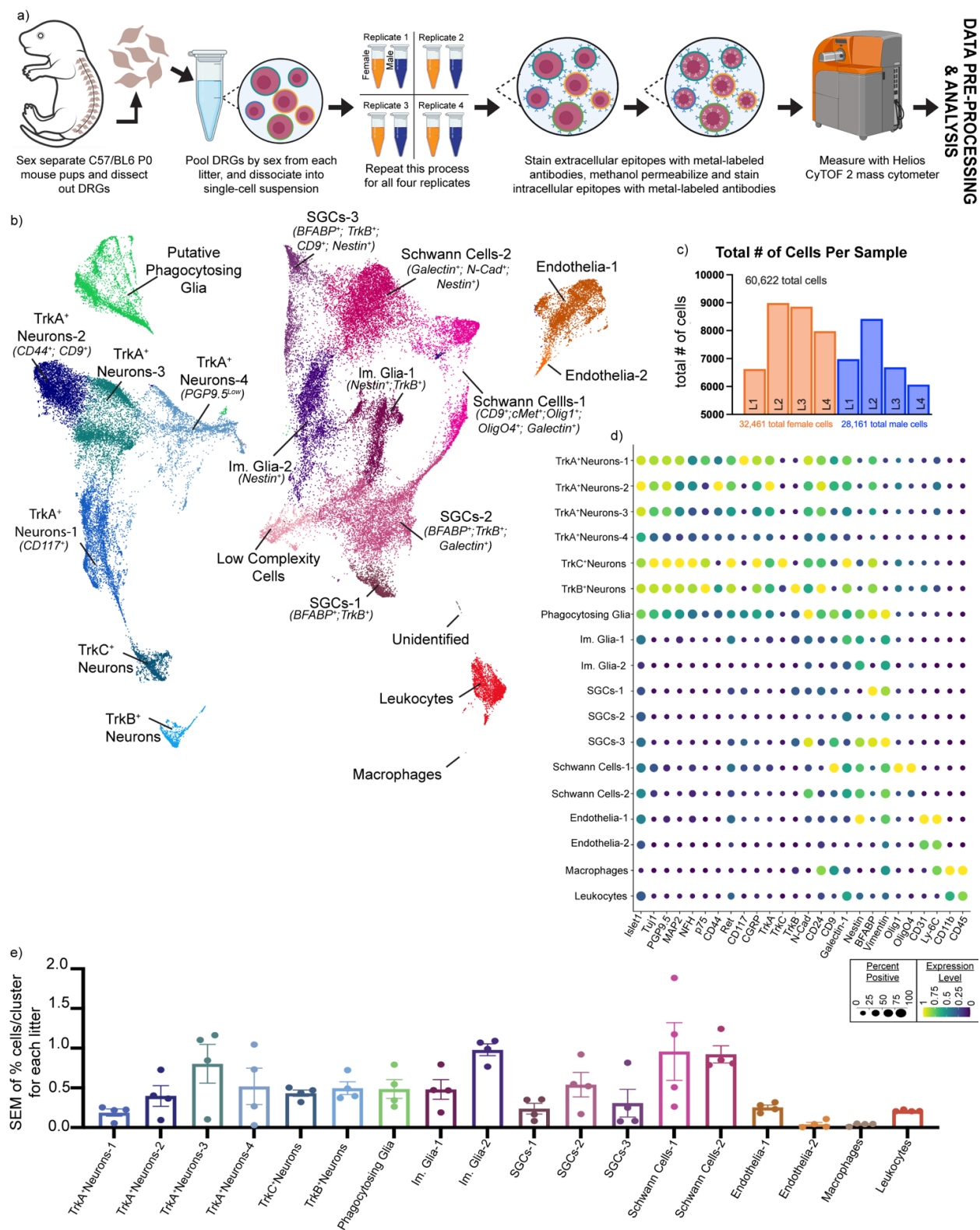


Fig. 3 Characterization of cell populations in the P0 mouse DRG by mass cytometry. a) Schematic depicting neural mass cytometry workflow. **b)** UMAP of all DRG cells present at P0

after preprocessing and hierarchical gating. Different colors represent different clusters determined by Leiden clustering and were identified and labeled as distinct cell populations according to differences in protein marker expression. **c)** The bar graph depicts the contribution from females or males from each of the four litters, “L_”, to the total 60,622 cells used for analysis in this and subsequent figures. **d)** Protein marker abundances across distinct cell types. The color of the dot indicates the relative expression level for each marker and the size of the dot represents the percentage of cells with positive expression for each marker within each cell population. **e)** Depiction of the standard error of the mean (SEM) calculated on the relative percentage of cells present for each litter in distinct clusters within the broad cell populations identified. The colors of the bars correspond to the color of the populations in the UMAP in subpanel (b).

Figure 4

a)

Litter #	Date Collected	Sex	# of Pups	Cell Count
1	2/21/21	Female	3	588,000
1	2/21/21	Male	4	936,000
2	3/8/21	Female	2	444,000
2	3/8/21	Male	4	1,280,000
3	3/9/21	Female	4	980,000
3	3/9/21	Male	4	931,000
4	3/11/21	Female	3	648,000
4	3/11/21	Male	5	1,120,000

b)

Metal	Antibody	Stock Conc. (ug/ml)	Staining Conc. (ng/ml)	Staining Location	Cell Type	Antibody Clone	Manufacturer	Product #
Pd102	Barcode - 1	100uM	50nM-1uM	Barcode	Sample ID	NA	Trade Sciences International	NA
Pd104	Barcode - 2	100uM	50nM-1uM	Barcode	Sample ID	NA	Trade Sciences International	NA
Pd105	Barcode - 3	100uM	50nM-1uM	Barcode	Sample ID	NA	Trade Sciences International	NA
Pd106	Barcode - 4	100uM	50nM-1uM	Barcode	Sample ID	NA	Trade Sciences International	NA
Pd108	Barcode - 5	100uM	50nM-1uM	Barcode	Sample ID	NA	Trade Sciences International	NA
Pd110	Barcode - 6	100uM	50nM-1uM	Barcode	Sample ID	NA	Trade Sciences International	NA
Y89	Tau1 (Beta III Tubulin)	0.2	1500	Intracellular	Neuron	Tau1J	Covance	MMS-435P-250
h113	GFAP	0.02	100	Intracellular	Glia	4A11, 1B4, 2E1	BD Biosciences	556330
h115	oMx	0.1	1000	Intracellular	Glia, Neurons	3D4	ThermoFisher	37-0100
La139	Substance P	0.2	200	Intracellular	Neuron	Polyclonal	Invitrogen	PA5-75165
Pr141	TrpV1	0.05	300	Surface	Neuron	Polyclonal	Novus	NBP1-71774
Nd142	CD9 (Hspa29)	0.2	300	Surface	Glia, Neuron	KM3B	BD Biosciences	564234
Nd143	CD117 (c-kit)	0.05	300	Surface	Neuron	2B8	Biologend	105802
Nd144	Nestin	0.002	30	Intracellular	Neural Stem Cells	307501	R&D Systems	MS2736
Nd145	NFR1 (CD120a)	0.02	300	Surface	Neuron		Biologend	MA5414
Sm147	NFH (Neurofilament H)	0.05	100	Intracellular	Neuron	NF-01	Novus	NB50-416
Nd148	CD133 (Prominin 1)	0.05	300	Surface	Stem Cell	315-2C11	Biologend	141202
Sm149	CD6P	0.05	1000	Intracellular	Neuron	Polyclonal	Bo-Rad	1720-9007
Nd150	TrkC	0.05	100	Surface	Neuron	Polyclonal	R&D Systems	AF1404
Eu151	Sox10	0.2	3000	Intracellular	Neural Crest Cells	NA	Gift from Dr. Sarah Kucenas	NA
Sm152	Ki67	0.5	2000	Intracellular	Proliferative Cells	B56	BD Biosciences	556003
Eu153	Olig2	0.2	1000	Surface	Glia	G4	R&D Systems	MBR1526
Sm145	Vimentin	0.05	100	Intracellular	Stem Cell, Glia	W16220A	Biologend	699302
Gd155	CD31 (PECAM-1)	0.05	100	Surface	Endothelia	390	Biologend	102425
Gd156	NeuroD1	0.2	1000	Intracellular	Neural Stem Cells	Polyclonal	R&D Systems	AF2746
Gd157	CD45 (PTRC)	0.002	10	Surface	Leukocytes	30-F11	Biologend	103102
Gd158	CD11b	0.05	100	Surface	Leukocytes/Macrophages	M170	Biologend	101249
Yt159	CD24	0.01	30	Surface	Neurons	M189	BD Biosciences	557436
Gd160	Sox2	0.2	1000	Intracellular	Neural Crest Cells	24810	R&D Systems	MB52018
Dy161	N-Cadherin (CD325/CDH2)	0.2	200	Surface	Neuron	13A9	Biologend	844702
Dy162	Galectin-1	0.1	300	Surface	Glia, Neurons	Polyclonal	R&D Systems	AF1245
Dy163	Calbindin D-28K	0.2	1000	Intracellular	Neuron	4H7	Novus	NBP2-50048
Dy164	MAPP	0.2	500	Intracellular	Neuron	4H5	Novus	NBP2-25156
Ho165	TrA	0.5	1000	Surface	Neuron	Polyclonal	Millipore-Sigma	06-574
Er166	Ly-8C	0.01	30	Surface	Macrophages	HK1.4	Biologend	128002
Er167	hM1	0.2	1000	Intracellular	Neuron	Polyclonal	Novus	NBP2-14999
Er168	PDGFRa (CD140a)	0.02	100	Surface	Endothelia	AP45	Biologend	135902
Tm169	Ret	0.5	2000	Surface	Neuron	Polyclonal	NeuroMics	GT15002
Er170	Gli3	0.005	30	Surface	Glia	G1	R&D Systems	MBR1527
Yb171	CD44	0.005	30	Surface	Neuron	IM7	BD Biosciences	553131
Yb172	BFABP (BLBP/FABP7)	0.5	2000	Intracellular	Glia	NA	Gift from C. Birchmeier and T. Mueller; Kurtz et al., 1994	NA
Yb173	CC3 (Cleaved Caspase 3)	0.2	500	Intracellular	Apoptosis	C92-805	BD Biosciences	556565
Yb174	TrkB	0.05	100	Surface	Neuron	Polyclonal	R&D Systems	AF1494
Lu175	PCP9.5	0.05	100	Intracellular	Neuron	Polyclonal	Millipore-Sigma	AB1761-I
Lu176	p75NTR (NG2R/NFRSF16)	0.005	10	Surface	Neuron	Polyclonal	R&D Systems	AF1167-I
Ox180	IS4	0.2	300	Surface	Neuron, Leukocytes	NA	Millipore-Sigma	AF1916
Pl918r193	DNA Intercalator	125uM	25nM	Post-stain	DNA	NA	Fluidigm	201192A
Pl195	Cisplatin	10uM	5uM	Pre-fix	Viability	NA	Sigma Aldrich	P4394

Fig. 4 Sample collection and antibody panel information. a) Table describing date of DRG collection, sex, number of pups, as well as raw cell count before staining for each of the four litters. Information for female pups is highlighted in orange and information for male pups is

highlighted in blue. **b)** Table containing information about the antibodies used for the DRG mass cytometry panel including the metal the antibody was conjugated onto, stock and staining concentrations, staining localization, antibody clone, manufacturer, and product number.

Figure 5

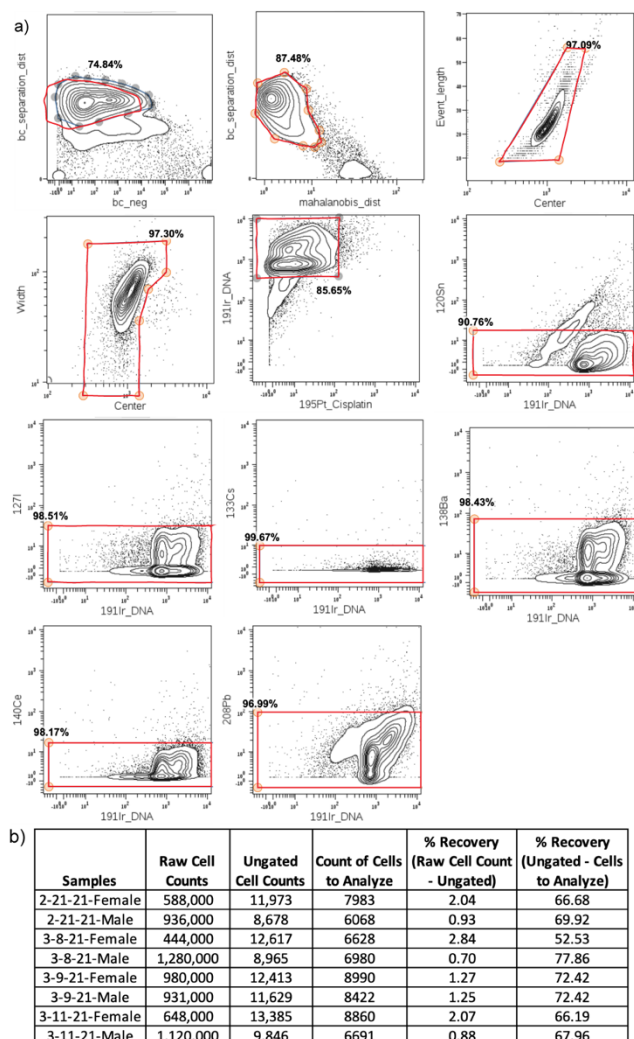


Fig. 5 Sample gating prior to high dimensional analysis. a) Biaxial gates demonstrating the clean-up gating done in Cytobank (community.cytobank.org). This clean-up gating was done to remove debris with low-DNA, rare metal aggregates, and cell doublets^[45] and is not a representation of population gating. Representative images were taken from the female sample

collected on 3/11/21. **b)** Table describing the raw cell counts before staining, after staining in the ungated population, and after gating in the cells to analyze population for each sample. Additionally, the percentage of cells recovered after staining and after gating were reported in the table.

Sex Differences in Relative Cell Abundance for Broad DRG Cell Types

To visualize sex differences in early postnatal DRG cell populations, we calculated the relative abundance of female to male cells at each 2-dimensional bin in the UMAP plot (see Materials and Methods) (Fig. 6a). In this abundance comparison UMAP, subsets of neuronal and putative phagocytic glial populations are proportionally more abundant in females (orange), subsets of the endothelial and glial populations are proportionally more abundant in males (blue), and regions with similar or identical female and male abundance appear gray in color. These gray regions with the highest similarity between the sexes largely correspond to the highest cell densities on the UMAP plot (Fig. 6b), but some high-density regions also skew toward female or male (e.g., TrkB⁺ neurons), and the non-random distribution in many low-density regions indicates that these observed differences in female-to-male abundance are not simply due to stochastic noise.

We next sought to quantitatively assess sex differences in specific somatosensory cell types. As Leiden clustering separated cell populations at a higher resolution than generalized canonical cell types, we first combined the clusters that represented each broad cell type to compare relative cell type abundances between female and male replicates. For the immune cells (combined leukocytes and macrophages), there were no significant differences in relative cell abundances between sexes (Fig. 6c), but we observed a significant increase in the relative abundance of male endothelial cells ($p=0.0239$) (Fig. 6d), a trending increase in male glial cells ($p=0.0512$) (Fig. 6e), and a significant increase in female combined neuronal populations

($p=0.0266$) (Fig. 6f) confirmed by IHC ($p=0.0194$) (Fig. 6m, n). The average relative abundance in each replicate for all populations within females and males is shown in Figure 6g.

In addition to relative abundance within these broad populations, variance was also examined. Similar to Figure 3d, SEM was calculated on the relative percentage of cells present for each cluster between males and females for leukocytes/macrophages (Fig. 6h), endothelial cells (Fig. 6i), glial cells (Fig. 6j), and neuronal cells (Fig. 6k). The SEM was also calculated on the combined relative percentage of cells for each general cell population for males and females (Fig. 6l). The SEM in the leukocytes/macrophages and endothelial cells is below 0.2 and displays negligible difference between males and females. In contrast, the variability in the neuronal and glial populations is much larger, with SEM values between 0.5 and 2, and does show sexual dimorphism in terms of which sex has more variability within their neuronal and glial populations. Females displayed higher variability in neuronal populations, while males displayed higher variability in glial populations.

Figure 6

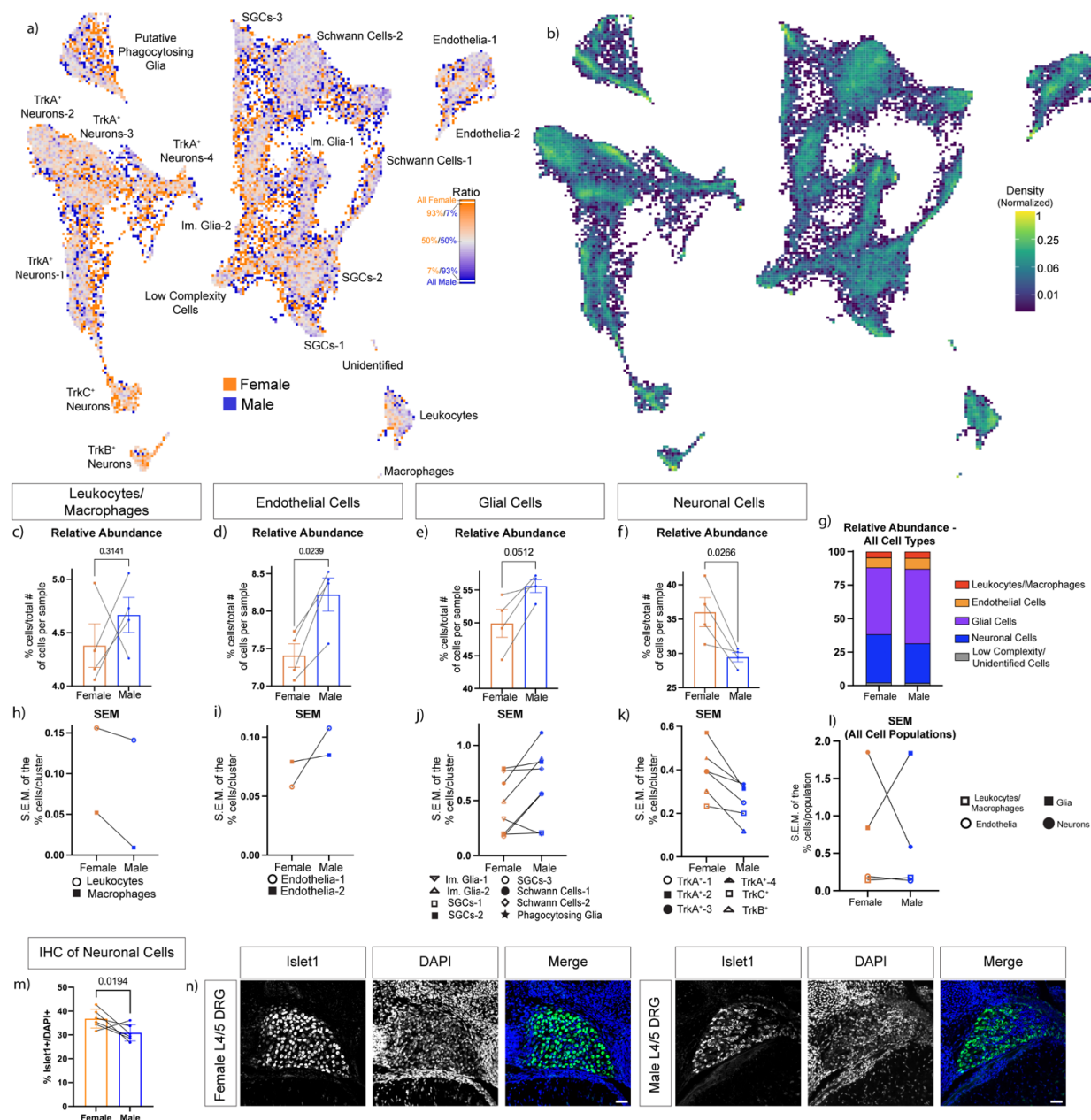


Fig. 6 Sexual dimorphism within general cell populations in the DRG. a) Relative abundance UMAP of all cells colored by which sex has the highest relative abundance for each bin. **b)** Density UMAP showing the normalized density of cells within each bin. **c-f)** Graphs depicting the relative abundance in female and male pups of the four general cell populations identified in Fig 3 – leukocytes/macrophages (c), endothelial cells (d), glial cells (e), and

neuronal cells (f). **g**) Stacked bar graph depicting the average relative abundance for all females and all males colored by the different cell types. Low complexity and unidentified cells were included in this graph and are colored in gray. **h-k**) Graphs depicting the SEM of the relative percentage of cells present for each male and female sample in distinct clusters within each cell population – leukocytes/macrophages (h), endothelial cells (i), glia (j), and neurons (k). **l**) Depiction of the SEM calculated on the combined relative percentage of cells for each male and female sample within the different clusters that form the four broad cell populations. **m**) Proportion of Islet1⁺ cells out of all DRG cells (DAPI⁺) by IHC. One to eight DRG sections were imaged and analyzed for up to two animals per litter for six litters for each sex. Counts from all sections from a single litter were averaged. **n**) Representative IHC images of P0 L4/L5 DRGs with anti-Islet1 and DAPI quantified in (m). Scale bar = 50µm Bins = 200 for subpanels (a) and (b). Connecting lines in subpanels (c)–(f) and (h)–(m) signify females and males from the same litter.

Figure 7

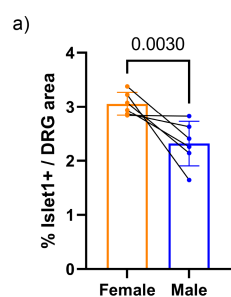


Fig. 7 Alternative analysis of neuronal proportion between sexes. a) Proportion of Islet1⁺ cells out of DRG area. DAPI staining in glia was small and tightly packed and overlapping. Cell counts may be unreported. While the proportion of Islet1⁺ by DAPI⁺ is a more similar comparison to the mass cytometry, we thus included Islet1⁺ by DRG area as an additional

comparison. Similar to both mass cytometry and Islet1⁺ by DAPI⁺, female DRGs exhibited a significant increase in the proportion of Islet1⁺ cells by DRG area.

Lack of Sex Differences in DRG Glial Populations

While examining multiple cell populations clustered together provides a broad view of sex differences that might exist in disparate cell types, it does not provide a clear picture of what might be occurring in more specific and specialized cell populations. To gain a clearer picture of how sex impacts distinct glial cell populations, we grouped cells expressing Vimentin, BFABP, Olig1, and/or OligO4 from our initial round of clustering (Fig. 8a inset), and reclustered these cells (e.g., secondary clustering). This resulted in the identification of 15 distinct glial clusters plotted on the UMAP in Fig.8a. Based on their protein expression, these clusters were defined as immature glial cells (Im. Glia), satellite glial cells (SGCs), Schwann cells, and putative phagocytosing glia (Fig. 8b). Broadly, immature glia were Vimentin⁺ with Nestin⁺ and/or Galectin-1⁺ subtypes. Satellite glial cells (SGCs) were BFABP⁺ with Nestin⁺ and/or TrkB⁺ subtypes. Schwann cells were Olig1⁺, OligO4⁺, and CD9⁺ with Nestin⁺ subtypes. Additionally, Schwann cell progenitors (Schwann cells-3) were N-cadherin⁺. Previous work has shown that during early development, glial precursor cells can phagocytose debris until macrophages fully infiltrate and act as the primary phagocytic cells^[40]. Additionally, previous work from our research group identified and characterized these putative phagocytic glia by mass cytometry in the DRG, finding nuclear protein expression representative of both neuronal and glial DRG populations, and DNA intercalator levels that imply these putative phagocytic events are not simple cell doublet artifacts^[45]. However, it is important to note that although there is some evidence from the literature that phagocytosis by immature satellite glia can occur in the DRG, this appears to occur at a higher frequency during embryonic development and was observed at lower frequency in P0 DRG. Therefore, we cannot rule out the possibility that our observations include a mixture of artifactual cell doublets or aggregates in addition to true phagocytic events.

Because of this, we refer to this cell population as putative phagocytosing glia, identified by their co-expression of the glial markers Vimentin and BFABP with the neuronal markers Islet1, MAP2, PGP9.5 and/or TuJ1.

To assess sexual dimorphism in neonatal glial populations, we generated a relative abundance UMAP (Fig. 8c). Generally, the Schwann cell populations have a slightly higher relative abundance in males, while the immature and putative phagocytosing glial populations have a slightly higher relative abundance in females. Similarly to Figure 6a, regions of the abundance UMAP with the higher relative abundance of females/males seems to be greater in less dense areas while the higher density areas of the UMAP have a distribution of female to male relative abundance values that are closer to 50/50 (Fig. 8c inset). Sex differences in the relative abundance of the four broad classes of glia identified in Fig. 8a were quantified (Fig. 8d). No significant sex differences were found in the relative abundance of any of these glial populations.

Figure 8

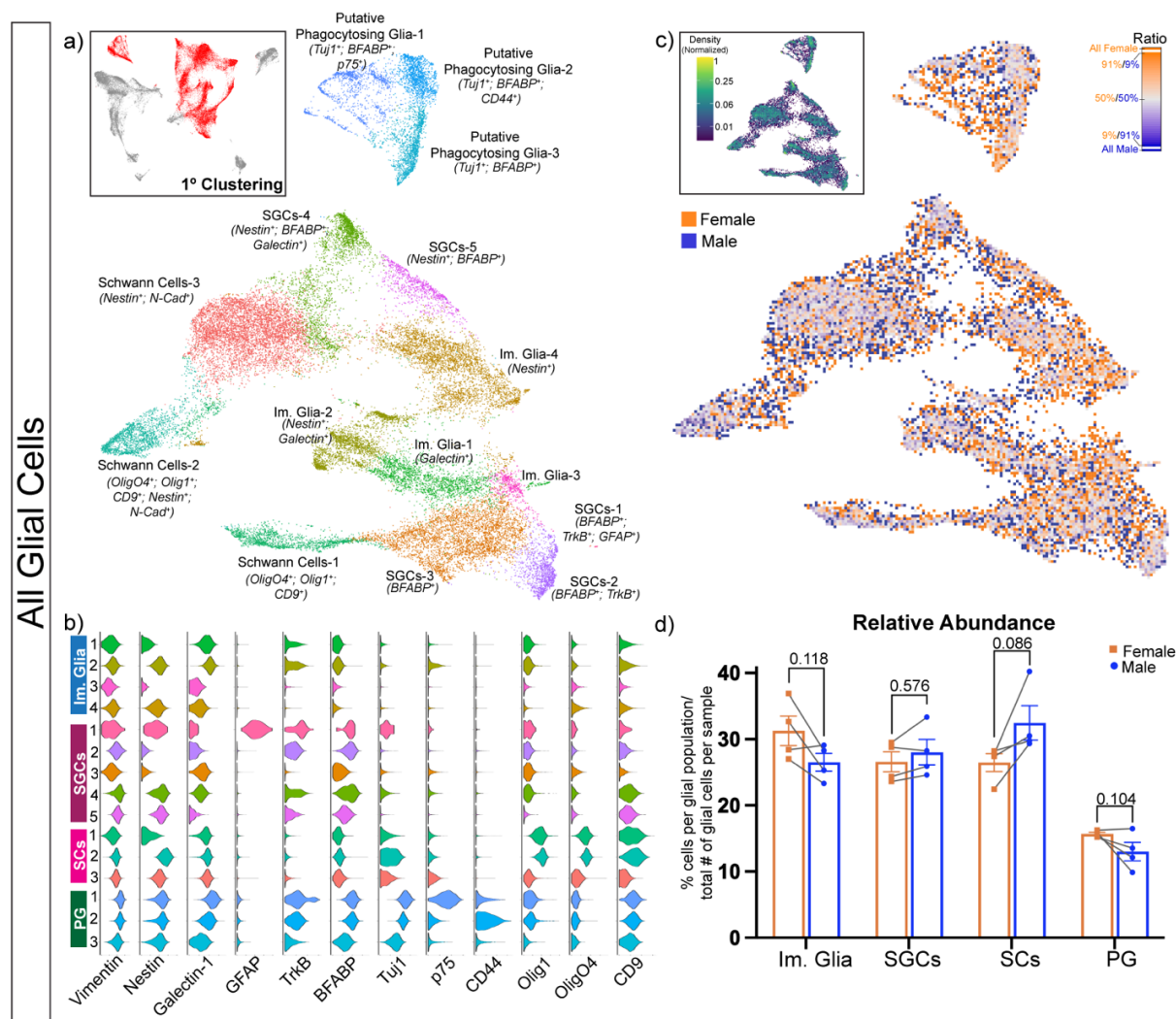


Fig. 8 No significant difference in the relative cell abundance of DRG glial classes. **a)** Cells identified as glia in Fig. 3b (shown in the inset highlighted in red) were extracted and re-clustered. The resulting UMAP contains 15 clusters that were identified as immature glia (Im. Glia), satellite glial cells (SGCs), Schwann Cells (SCs) or putative phagocytosing glia. **b)** Violin plots for 12 key markers used for identifying distinct glial populations in subpanel (a). **c)** Relative abundance UMAP of all cells colored by which sex has the highest relative abundance for each bin. An inset of the density UMAP depicting normalized density of cells present within each bin is also included. **d)** Bar graphs depicting the relative abundance of cells for the four general glial populations (immature glia, satellite glial cells, Schwann cells, and putative phagocytosing glia)

with p-values listed above each set of bar graphs. No statistically significant differences were found between sexes for any of the glial populations when examining relative abundance. A total of 31,978 cells were analyzed in this figure. Bins = 200 for relative abundance UMAP and density UMAP in subpanel (c). Connecting lines in subpanel (d) signify females and males from the same litter.

We next conducted a tertiary round of clustering on only the immature and satellite glial cells (Fig. 9a inset). This resulted in 13 distinct clusters that are visualized in the UMAP in Fig. 9a. Clusters 1-6 are the immature glia identified primarily by their shared expression of Nestin with low expression levels of Sox 2 and/or Sox10 (Fig 9b). Cell populations and/or states were delineated by varying expression of CD24 and co-expression between Nestin, Sox2, Sox10, and CD24 to form specific subclusters (Fig 9b). Clusters 7-13 correspond to satellite glial cells primarily identified by BFABP and TrkB expression (Fig 9b). Specific subclusters were determined by variable expression of Nestin, Galectin-1, CD24, CD9, CD117, and GFAP (Fig 9b). An abundance UMAP was generated (Fig. 9c) and the relative abundance of each cluster for males and females was quantified (Fig. 9d). No significant sex differences exist in any of the distinct cell populations or states represented in each cluster (Fig. 9d). Tertiary clustering and sex difference analysis was also conducted on Schwann cells (Fig. 9e inset) which resulted in the identification of 7 distinct clusters (Fig. 9e). Clusters 1-4 correspond to immature/non-myelinating Schwann cells, while clusters 5-7 represent mature/myelinating Schwann cells (Fig. 9f). An abundance UMAP was generated (Fig. 9g) and the relative abundance of each cluster for males and females was quantified (Fig. 9h). No statistically significant differences were found between males and females for any of the specific cell types and states in each cluster (Fig. 9h). These findings suggest that somatosensory glial abundance is not sexually dimorphic at P0.

Figure 9

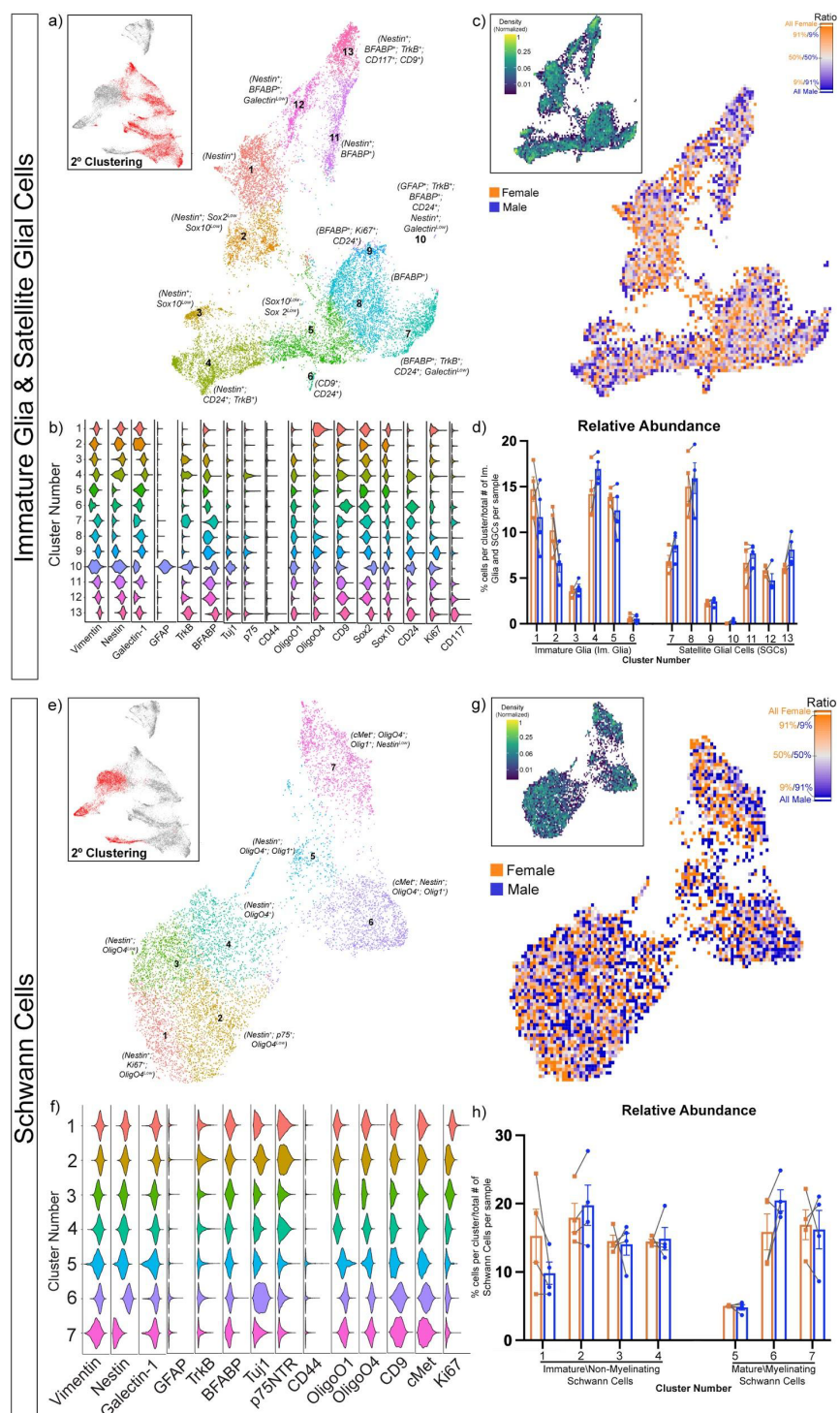


Fig. 9 No significant difference in the relative cell abundance of DRG glial subtypes.

Tertiary clustering was conducted for the immature glia and SGCs (a-d), as well as Schwann cells (e-h). **a,e)** UMAP of extracted and reclustered cells that were identified as immature glia

and satellite glial cells (a) or Schwann cells (e) from secondary clustering of glia (shown in inset with extracted cells highlighted in red). More specific cell states and populations were identified by marker expression which can be seen in the annotations on the UMAPs and violin plots (b,f). **c,g**) Relative abundance UMAP of all cells colored by which sex has the highest relative abundance for each bin for immature glia and satellite glial cells (c) or Schwann cells (g). **d,h**) Bar graphs depicting relative cell abundance for each cluster determined for immature glia and satellite glial cells (d) or Schwann cells (h). A total of 17,977 cells in subpanels (a-d), and 9,447 cells in subpanels (e-h). Bins = 200 for relative abundance UMAP and density UMAP in subpanel (c), (g). Connecting lines in subpanels (d), (h) signify females and males from the same litter.

Figure 10

a) Im. Glia & SGCs		b) Schwann Cells	
Cluster #	p-value	Cluster #	p-value
1	0.24	1	0.24
2	0.07	2	0.63
3	0.5	3	0.81
4	0.15	4	0.82
5	0.35	5	0.61
6	0.86	6	0.18
7	0.13	7	0.85
8	0.71		
9	0.55		
10	0.06		
11	0.43		
12	0.2		
13	0.07		

Figure 10 **p-values for relative abundance bar graphs for glial populations.** **a)** Table containing the p-value for each of the immature glial and satellite glial cell clusters represented in the relative abundance bar graph. **b)** p-values for each of the Schwann cell clusters represented in the relative abundance bar graph.

Sex Differences in TrkA⁺, TrkB⁺, and TrkC⁺ neurons

To gain a clearer picture of how sex impacts distinct neuronal cell populations, we extracted cells from our initial round of clustering expressing Islet1, TuJ1, PGP9.5, TrkA, TrkB, and/or TrkC with low levels of the glial markers Vimentin and BFABP (Figure 5a inset), and reclustered these, resulting in 9 distinct secondary clusters. One low complexity cluster constituting approximately 4% of all neuronal cells was removed from the UMAP as well as from all subsequent abundance calculations (data not shown). The remaining 8 clusters corresponding to 5 distinct neuronal subpopulations were plotted on the UMAP shown in Figure 11a. Trk receptor expression generally characterizes three broad neuronal populations in the DRG – nociceptors (TrkA⁺), mechanoreceptors (TrkB⁺), and proprioceptors (TrkC⁺). Nociceptor subtypes are divided into general (TrkA⁺, MAP2^{low}), non-peptidergic (TrkA⁺, CD9^{+/-}, CD44^{+/-}, Galectin-1^{+/-}), and peptidergic (TrkA⁺, CD117⁺, CD9^{+/-}, NFH^{+/-}) (Fig. 11b)[2,2,45]. TrkB⁺ and TrkC⁺ neurons were also able to be identified by their respective Trk expression (Fig. 11b). The relative abundance UMAP revealed several qualitative differences, with female cells predominating TrkB⁺ and TrkC⁺ clusters while TrkA⁺ nociceptors appeared to be increased in males (Fig. 11c). Quantification of these differences show that females have a larger relative abundance of TrkB⁺ and TrkC⁺ neurons while males have a larger relative abundance of TrkA⁺ neurons (Fig. 11d). When examining TrkA⁺ nociceptors more specifically, we found no significant sex differences in the relative abundance of general or non-peptidergic nociceptors. However, peptidergic nociceptors have a larger relative abundance in males when compared to females (inset of Fig. 11d). The relative abundance of TrkA⁺ and TrkC⁺ neurons were confirmed by IHC (Fig. 11e,f), however, the satellite glial cells ensheathing neurons have high expression of TrkB⁺ preventing a similar analysis.

Figure 11

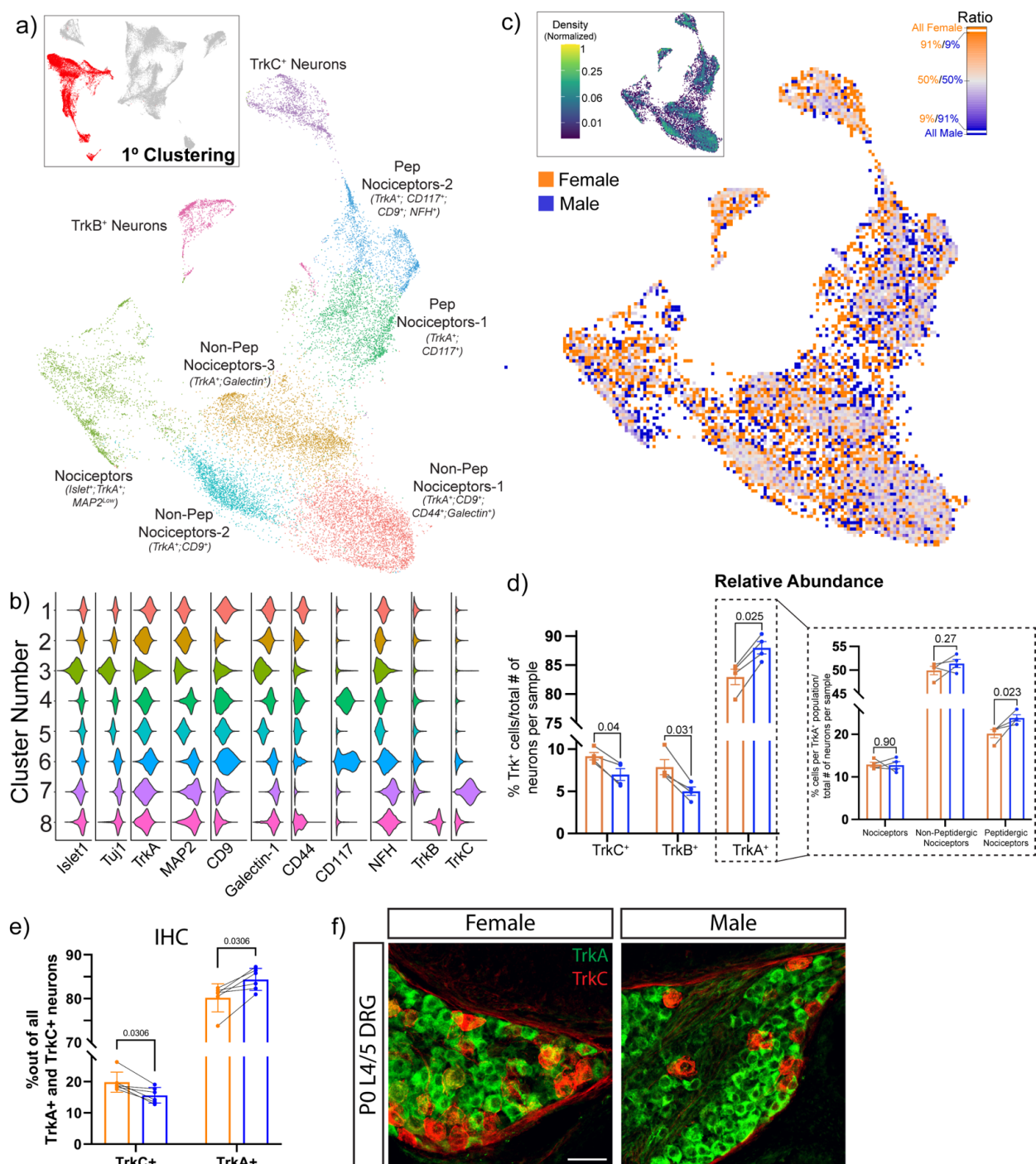


Fig. 11 Sexual dimorphism in neuronal classes. **a)** Cells identified as neurons in Fig. 3b (shown in the inset highlighted in red) were extracted and re-clustered. The resulting UMAP originally had 9 clusters, of which, one was identified as low complexity and removed from the UMAP as well as all subsequent analysis (data not shown). The 8 remaining clusters can be

further identified by protein expression and divided into 5 subpopulations – general nociceptors, non-peptidergic nociceptors, peptidergic nociceptors, TrkB⁺ neurons, and TrkC⁺ neurons. **b)** Violin plots for 11 key markers used for identifying distinct neuronal populations in subpanel (a). **c)** Relative abundance UMAP of all cells colored by which sex has the highest relative abundance for each bin. An inset of the density UMAP depicting normalized density of cells present within each bin is also included. **d)** Bar graph depicting the relative abundance of 3 general neuronal subpopulations identified by Trk expression. For TrkA⁺ neurons, 3 specific subpopulations were identified, and the relative abundance was recalculated for general, non-peptidergic, and peptidergic nociceptors. **e)** Proportion of TrkA⁺ or TrkC⁺ cells out of all TrkA⁺ and TrkC⁺ cells by IHC. One to seven DRG sections were imaged and analyzed for up to two animals per litter for six litters for each sex. Counts from all sections from a single litter were averaged. **f)** Representative IHC images of P0 L4/L5 DRGs with anti-TrkA and anti-TrkC quantified in (e). Scale bar = 30µm. A total of 19,073 cells were analyzed for subpanels (a)-(d). Bins = 150 for relative abundance UMAP and density UMAP in subpanel (c). Connecting lines in subpanels (d) and (e) signify females and males from the same litter.

The Impact of Sex on Distinct Cell States and Populations Within TrkA⁺ Neuronal Subpopulations

We next sought to investigate distinct cell types/states within the subpopulations defined in Fig 11. To that end, we extracted non-peptidergic nociceptors from our secondary round of clustering (Figure 12a inset) and conducted a tertiary round of clustering on these specific cells. This resulted in the identification of 9 distinct clusters which were plotted on the UMAP in Figure 11a. Molecular distinction between the specific clusters was determined by expression of specific markers with violin plots (Fig. 12b). Visualization of sex differences are shown with the abundance UMAP (Fig. 12c). For analysis of relative abundance within specific cell subtypes, the abundance is normalized within that specific subtype. Sex differences in the relative

abundance of cells for each distinct cluster were analyzed and no statistically significant differences exist between males and females in any cluster for the non-peptidergic nociceptors (Fig. 12d). We repeated this analysis for peptidergic nociceptors and found only one statistically significant difference (Fig. 12e-12h). Putative immature peptidergic nociceptors in cluster 7, which are CD117⁺, p75 neurotrophin receptor (p75)⁺, and MAP2^{low}, had a significantly higher relative cell abundance (p=0.01) in females compared to males (Fig. 12h). Although peptidergic nociceptors have a greater relative abundance in males when examining neuronal populations generally, we see an increase in this subpopulation of peptidergic nociceptors in females after specific examination of these neurons. Of note for this and subsequent figures, significant sex differences in relative abundance of specific cell populations may differ or be masked by significant differences in more general cell populations (as seen in the peptidergic nociceptors).

Figure 12

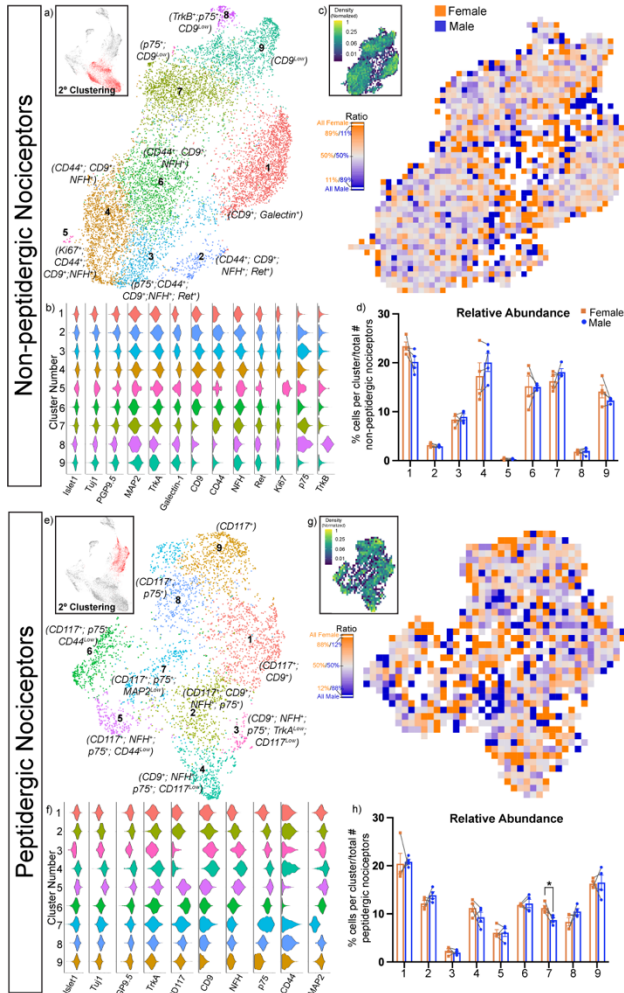


Fig. 12 Sexual dimorphism in nociceptive populations. a) UMAP of extracted and re-clustered cells that were identified as non-peptidergic nociceptors in Fig. 11a (shown in the inset highlighted in red). **b)** Violin plots for 13 markers used to identify distinct cell states within the non-peptidergic nociceptors for each cluster. **c)** Relative abundance UMAP of all cells colored by which sex has the highest relative abundance for each bin. An inset of the density UMAP depicting normalized density of cells present within each bin is also included. **d)** Bar graph depicting relative abundance of the 9 different clusters shown in subpanel a. **e-h)** UMAP (e), violin plots (f), relative abundance UMAP (g), and relative cell abundance per cluster (h) for peptidergic nociceptors. The peptidergic nociceptors were identified, extracted, and reclustered from the UMAP in Fig. 5a (shown in the inset highlighted in red in subpanel e) and analyzed as

described above for non-peptidergic nociceptors (a-d). A total of 9,658 cells were analyzed in subpanels (a-d), and 4,150 cells in subpanels (e-h). Bins = 50 for relative abundance UMAP and density UMAP in subpanel c and bins = 40 for subpanel (g). Connecting lines in subpanels (d) and (h) signify females and males from the same litter.

Figure 13

a) Non-Peptidergic Nociceptors		b) Peptidergic Nociceptors	
Cluster #	p-value	Cluster #	p-value
1	0.07	1	0.86
2	0.37	2	0.12
3	0.54	3	0.45
4	0.43	4	0.2
5	0.8	5	0.98
6	0.95	6	0.74
7	0.17	7*	0.01
8	0.69	8	0.09
9	0.22	9	0.9

Fig. 13 **p-values for relative abundance bar graphs for TrkA⁺ neuronal populations.** **a)** p-values for each of the non-peptidergic nociceptive clusters represented in the relative abundance bar graph. **b)** p-values for each of the peptidergic nociceptive clusters represented in the relative abundance bar graph.

The Impact of Sex on Distinct Cell States and Populations Within TrkB⁺ and TrkC⁺ Neuronal Subpopulations

We next performed similar analysis with tertiary clustering to compare subtypes of TrkB⁺ (Fig. 14a-14d) and TrkC⁺ neurons (Fig. 14e-14h). For TrkB⁺ neurons, two clusters showed statistically significant sex differences. In cluster 6 ($p=0.02$), which is MAP2^{low}, females had a higher relative abundance while in cluster 9 ($p=0.01$), which is CD117⁺, there is a higher relative abundance in males (Fig. 14d).

TrkC⁺ neurons had 3 distinct clusters that were significantly different between males and females. Clusters 1 and 7 had a higher relative abundance in females ($p=0.007$ and $p=0.04$, respectively). Both clusters are p75⁺ and CD24⁺, however, cluster 1 is MAP2^{high} while cluster 7 is MAP2^{low}. Conversely, cluster 4, which is characterized primarily by MAP2 expression, had a higher relative cell abundance in males ($p=0.008$) (Fig. 14h). Cluster 7 in the TrkC⁺ neurons has a larger relative abundance in females and is MAP2^{low}. A common theme amongst TrkB⁺ and TrkC⁺ UMAPs is that female cells tend to be overrepresented in MAP2^{low} clusters. While this may not represent a distinct cell type compared to other clusters in the UMAP, we have previously suggested that this may represent a distinct cell state (i.e. maturity)^[45], which will be discussed further below. Overall, we see that females seem to have a greater relative abundance of cells with low MAP2 expression over multiple neuronal subpopulations.

Figure 14

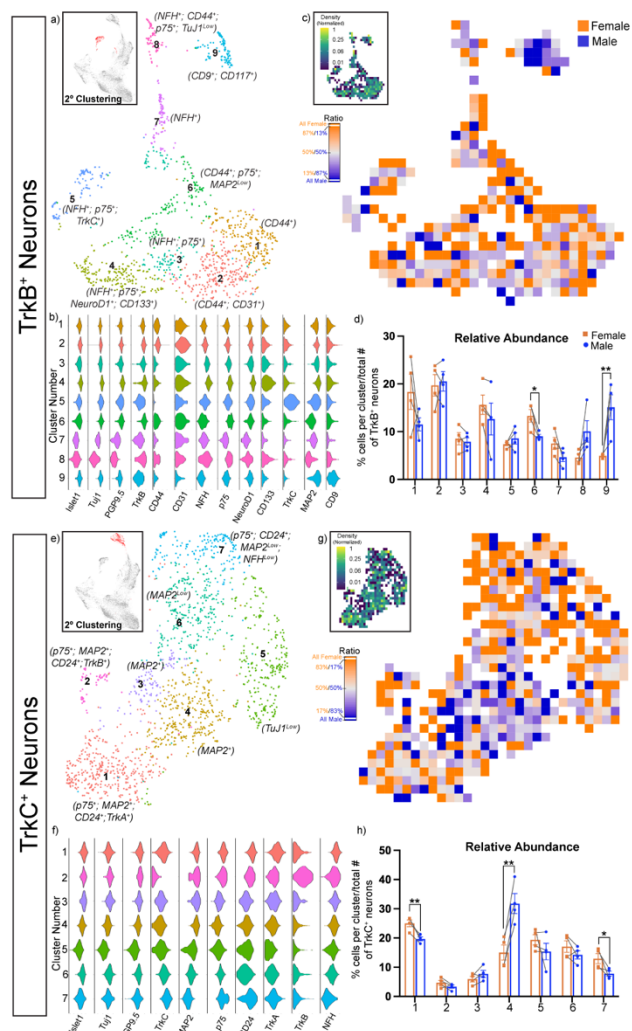


Fig. 14 Sexual dimorphism in TrkB⁺ and TrkC⁺ neuronal subtypes. **a)** UMAP of extracted and reclustered cells that were identified as TrkB⁺ neurons in Fig. 11a (shown in the inset highlighted in red). **b)** Violin plots for 13 key markers used to identify distinct cell states within each TrkB⁺ neuronal cluster. **c)** Relative abundance UMAP colored by which sex has the highest relative abundance for each bin. An inset of the density UMAP depicting normalized density of cells present within each bin is also included. **d)** Bar graph depicting relative abundance for the 9 different clusters shown in subpanel (a). **e-h)** UMAP (e), violin plots (f), relative abundance UMAP (g), and relative cell abundance per cluster (h) for TrkC⁺ neurons. TrkC⁺ neurons were identified, extracted, and reclustered from the UMAP in Fig. 5a (shown in the inset highlighted in red in subpanel (e) and analyzed as described above for non-TrkB⁺

neurons (a-d). A total of 1,262 cells were analyzed in subpanels (a-d), and 1,566 cells in subpanels (e-h). Bins = 30 for relative abundance UMAP and density UMAP in subpanels (c) and (g). Connecting lines in subpanels (d) and (h) signify females and males from the same litter.

Figure 15

TrkB ⁺ Neurons		TrkC ⁺ Neurons	
Cluster #	p-value	Cluster #	p-value
1	0.14	1*	0.007
2	0.8	2	0.24
3	0.68	3	0.28
4	0.47	4*	0.008
5	0.38	5	0.27
6*	0.02	6	0.29
7	0.11	7*	0.04
8	0.06		
9*	0.01		

Fig. 15 p-values for relative abundance bar graphs for TrkB⁺ and TrkC⁺ neuronal populations. **a)** p-values for each of the TrkB⁺ neuronal clusters represented in the relative abundance bar graph. **b)** p-values for each of the TrkC⁺ neuronal clusters represented in the relative abundance bar graph.

Putative Glial Phagocytosis Reflects Neuronal Sexual Dimorphism

We next examined the types of cargoes being consumed by putative phagocytosing glia. We conducted a tertiary round of clustering on the putative phagocytosing glial cells from Figure 8 (highlighted in red on the inset UMAP in Fig. 16a) and identified 9 distinct clusters (Figure 16a). In contrast to previous rounds of tertiary clustering, separation of clusters is mostly driven by the cargoes that the putative phagocytosing glia are consuming as opposed to intrinsic differences in glial subtype or state. To identify subsets of cargo types being consumed by putative phagocytosing glia, we examined the expression of 14 different markers with violin plots (Fig. 16b). In general, the phagocytosing subsets had varying abundance levels of the three Trk

receptors and most clusters were Nestin⁺. We used an abundance UMAP to visualize sex differences in relative abundance (Fig. 16c), and quantified relative cell abundance for each cluster (Fig. 16d). Significant sex differences were found in the relative abundance of clusters 1,3, and 9. Clusters 1 and 9 had a larger relative cell abundance in females ($p=0.04$ and $p=0.02$, respectively), while cluster 3 had a higher relative cell abundance in males ($p=0.03$). The sexual dimorphism seen in the debris consumed, aligns with the sexual dimorphism observed in the different neuronal subpopulations. Cluster 1, which has a higher relative abundance in females, is also MAP2^{low} which corresponds with our findings in Figures 5 and 6. Additionally, cluster 9, which also has a higher relative abundance in females, is TrkB⁺ which relates to our findings in Figure 11. Finally, cluster 3 has a larger relative abundance in males and is TrkA⁺ and Nestin^{low} which relate to the findings in Figures 11 and 12. These results indicate that the debris consumed by the putative phagocytosing glia correlates to the abundance of specific neuronal populations.

Figure 16

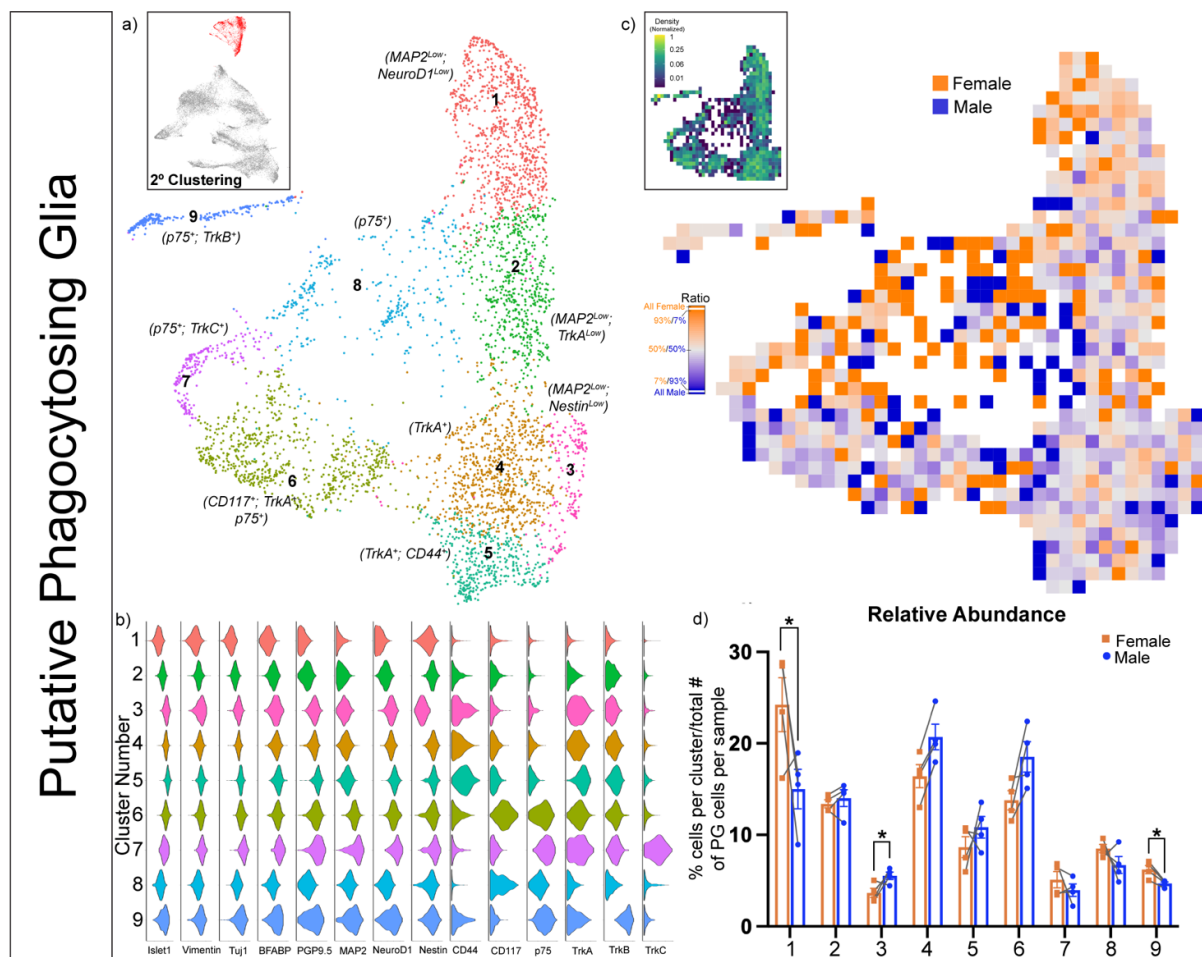


Fig. 16 Putative glial phagocytosis reflects neuronal sexual dimorphism. **a)** UMAP of extracted and reclustered cells that were identified as putative phagocytosing glia from secondary clustering of glia from Fig. 8a (shown in inset with extracted cells highlighted in red). **b)** Violin plots for 14 markers used to identify different debris consumed by the putative phagocytosing glia. **c)** Relative abundance UMAP colored by which sex has the highest relative abundance for each bin. An inset of the density UMAP depicting normalized density of cells present within each bin is also included. **d)** Bar graph depicting relative abundance for the 9 different clusters shown in subpanel a. A total of 4,554 cells were analyzed in this figure. Bins = 40 for both relative abundance and density UMAPs. Connecting lines in subpanel (d) signifies females and males from the same litter.

Figure 17

a)

Putative Phagocytosing Glia	
Cluster #	p-value
1*	0.04
2	0.56
3*	0.03
4	0.06
5	0.24
6	0.05
7	0.34
8	0.13
9*	0.02

Fig. 17 **p-values for relative abundance bar graphs for putative phagocytic glia.** a) p-values for each of the putative phagocytic glial clusters represented in the relative abundance bar graph.

Multi-Trk⁺ Neurons and Pseudotime Analysis Indicate a Developmental Delay in Female vs. Males for some Neuronal Subtypes

The overrepresentation of MAP2^{low} neurons in females implies a shift in maturity of select neuronal populations. We have previously shown that increased proportions of multi-Trk positive neuronal populations correlate with increased expression of immature and stem cell markers[45]. Based on these findings, we sought to test the notion that neuronal subtypes in females may be more molecularly immature by examining the relative abundance of each multi-Trk population out of all the Trk⁺ neurons. To assess the relationship of the cell subtypes, we analyzed the totality of the TrkA⁺ neurons, instead of breaking it down into peptidergic nociceptors and non-peptidergic nociceptors. In all three combinations of multi-Trk⁺ neurons, females consistently have a greater relative abundance, although only TrkA⁺/TrkC⁺ and

TrkB⁺/TrkC⁺ populations were statistically significantly increased (Fig. 18a). Next, we used URD pseudotime analysis to infer relative molecular maturity (pseudotime) of male and female Trk⁺ populations. Based on our previous work, we know maturational heterogeneity exists within a single time point during early DRG development^[45]. To examine sex differences in maturation within this data set, we first used molecular markers to identify which cluster was least mature (“root”) and which clusters were most mature (“tips”) for each Trk receptor (Fig. 18b).

Dendrograms were constructed which placed cells along the developmental trajectories from the root to tips for each Trk⁺ neuronal population. Dendrograms for each Trk receptor are colored so female cells are orange and male cells are blue (Fig. 18c, 18h, 18m). First, we examined the relative abundance of the cells with a pseudotime value of zero, which includes non-root cells in addition to manually selected root cells. This analysis compares the prevalence of sex difference in the most immature cells (Fig. 18d, 18i, 18n). The relative abundance of cells with a pseudotime value of 0 were elevated in females for TrkA⁺ and TrkB⁺ neurons and significantly increased in females for TrkC⁺ neurons ($p=0.02$). Although all three Trk⁺ receptors illustrate an increase in relative abundance of female cells with a pseudotime value of 0, the only statistically significant increase seen is in TrkC⁺ neurons ($p=0.02$). Histograms were generated depicting the relative number of female or male pseudotime values within each bin listed on the x-axis for all of the different segments (Fig. 18e, 18j, 18o). For all three Trk⁺ neuronal populations, the histograms depict female pseudotime values being shifted closer to a pseudotime value of 0, indicating decreased maturity. Lastly, we sought to examine how sexual dimorphism in pseudotime values differ between neuronal populations in each dendrogram. To determine which segments to examine further, we examined sex differences in the pseudotime value for each individual segment and determined if statistically significant differences existed (data not shown). The results of this analysis revealed that the C-LTMR neurons, primarily Tuj1^{low} that were identified by tertiary clustering of all TrkA⁺ neurons (data not shown), TrkB⁺-4 neurons, and TrkC⁺-5 neurons had statistically significant differences in the pseudotime values

between males and females with female pseudotime values being consistently lower (i.e. more immature) than male pseudotime values.

Figure 18

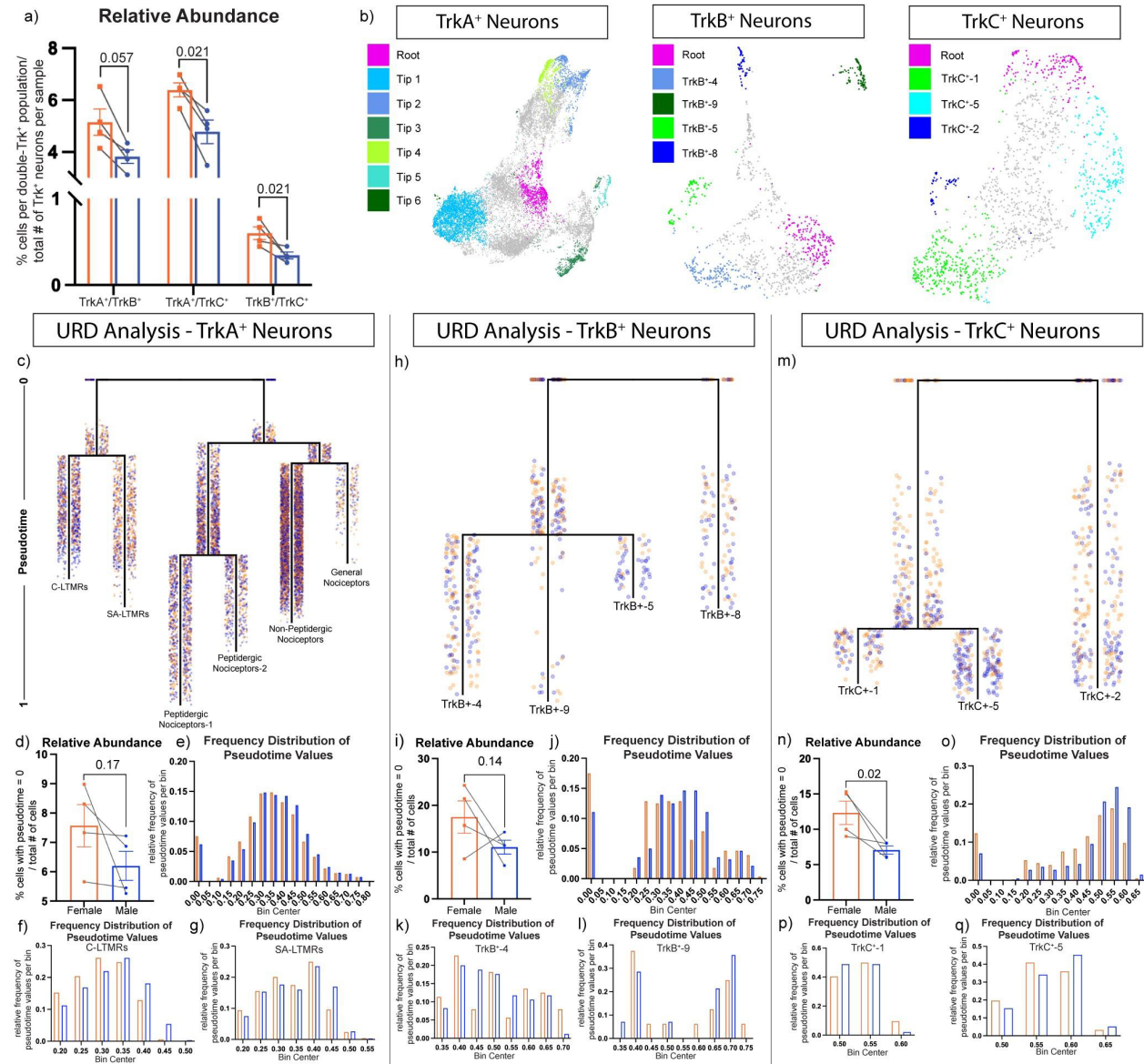


Fig. 18 Multi-Trk expression and pseudotime analysis indicate decreased maturity of neuronal populations in females at postnatal day 0. a) Bar graph depicting the relative abundance of multi-Trk⁺ populations determined by thresholding. b) UMAPs depicting which

cells were used as the root (magenta) and tips (green and blue shades) for URD analysis of all three Trk receptors. **c)** Dendrogram depicting pseudotime URD analysis for TrkA⁺ neurons. The cells were colored by sex and the tips were labeled with the TrkA⁺ neuronal populations they correspond to. **d)** Bar graph depicting the relative abundance of male or female cells that had a pseudotime value of zero, representing the root/most immature cells. **e)** Histogram depicting the number of female and male cells in each bin corresponding to the pseudotime value generated by URD analysis for all segments of the dendrogram. A pseudotime value closer to 0 represents more immature cells, while a pseudotime value closer to 1 represents more mature cells. **f,g)** Histograms depicting the number of female and male cells in each bin for the neuronal populations that correspond to the first two tips on the dendrogram in subpanel c. The dendrogram from URD analysis, bar graph depicting relative abundance of cells with a pseudotime value of 0, histogram of the relative frequency of pseudotime values for all segments, and the histograms depicting the relative frequency of the first two tips on the dendrogram were generated for TrkB⁺ (**h-l**), and TrkC⁺ (**m-q**) neurons. Connecting lines in subpanels (a), (d), (i), and (n) signify females and males from the same litter.

2. 5 Discussion

In this study, we examined whether the abundance of glial and neuronal populations within the P0 DRG are sexually dimorphic. We found no differences in immature glia, SGCs, or Schwann cells, but did observe statistically significant sexual dimorphism in the relative abundances of TrkA⁺, TrkB⁺, and TrkC⁺ neuronal populations both broadly and within more distinct subpopulations, as well as in the relative abundances of putative phagocytosing glia. Finally, examination of multi-Trk⁺ neuronal populations as well as URD pseudotime analysis indicates that specific female sensory neuron populations are less mature than males (Fig. 19).

Figure 19

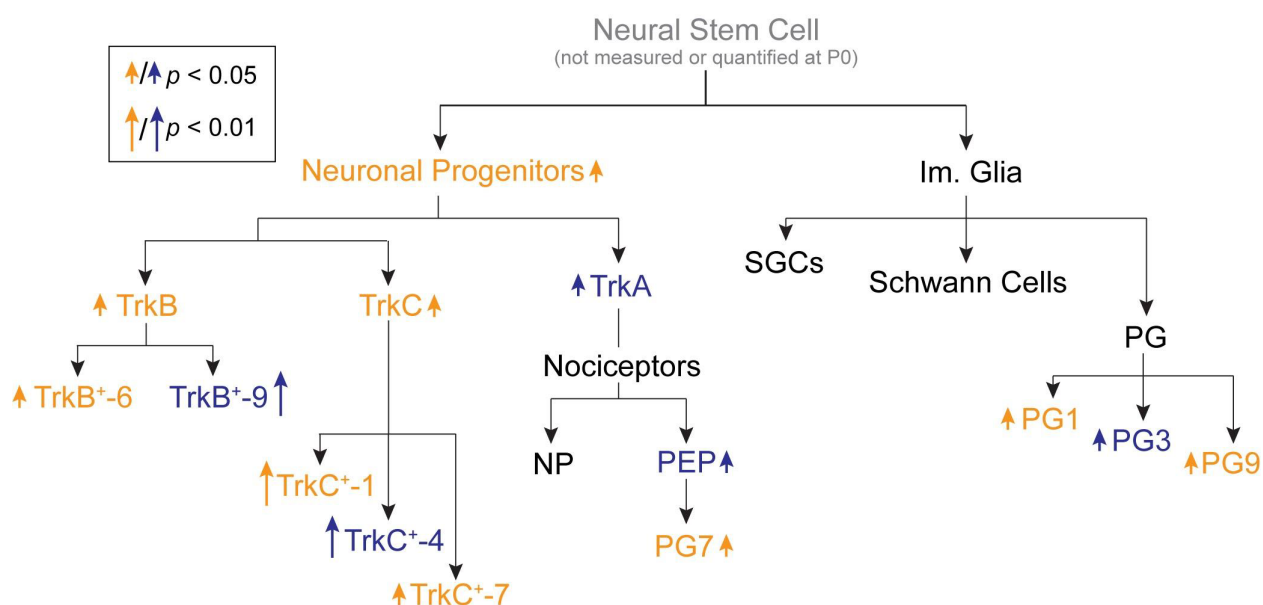


Fig. 19 **Sexual dimorphism through somatosensory development in the DRG at P0.** Male and female relative abundance changes per cell type are indicated by upward arrows with orange text denoting greater abundance in females and blue text denoting greater abundance in males. Gray text was not measured in this current study. The size of the arrow is correlated with the level of significance.

Most studies that have analyzed the DRG by scRNA-seq or mass cytometry did not separate by sex, and those that did were limited by a lack of sample replicates, precluding the identification of statistically significant differences in the composition of somatosensory cell types between females and males^[2,17,45,60,61]. Instead, previous single-cell studies have either combined sexes for pooled analysis, or only examined males. This represents a blind spot in the published literature, which we begin to address with this study. One example motivating this work is that established analgesics have been shown to be more efficacious in males than females in both humans and mice^[105,114,123]. This observation is not surprising given that the initial studies validating these analgesics relied on male mice. In this study we find that P0 females have a

higher relative abundance of TrkB⁺ and TrkC⁺ neurons, while males showed larger relative abundance of TrkA⁺ peptidergic nociceptive neurons (Fig. 11d). One potential explanation for differential efficacy of established analgesics could relate to our findings of increased relative abundance for specific nociceptor subtypes in males. However, given that various other factors could contribute to the decreased efficacy of some analgesics in females, it will be essential for our group and others to (1) examine whether these differences in cell abundance persist into adulthood, (2) whether there are sexually dimorphic differences in the molecular targets for established analgesics (e.g. opioid receptor) within neuronal subpopulations, and (3) whether the electrophysiological properties of nociceptor subpopulations are different between the sexes.

In addition to sexual dimorphism observed in neuronal populations, we also observed female-male differences in the cargoes consumed by the putative phagocytosing glia. This is reminiscent of the increase in phagocytic microglia in females in the brains of postnatal day 2 mice, a difference that is not observed at earlier time points^[87]. Interestingly, these microglia appear to engulf immature neurons. In the peripheral nervous system, immature SGCs are key phagocytes that engulf developmental debris before macrophage infiltration^[40,45,132]. Our previous mass cytometry analysis found that phagocytic SGCs begin to emerge around embryonic day (E) 13.5, peak around E15.5, and are drastically reduced by P4, which corresponds to how neurons are initially overproduced during development, resulting in the eventual pruning and death of approximately 50% of the original neurons generated^[45,133]. In this study, we observed that at P0, compared to male counterparts, putative female phagocytic SGCs preferentially engulf MAP2^{low} presumptive immature neurons (Fig. 16d). Unsurprisingly, this is proportional to the relative difference in abundance between male and female immature neurons. An important caveat to this result is that some of these cells we categorize as putative phagocytosing glia could instead be artifactual cell doublets or aggregates. To address this

concern, we previously performed phase contrast microscopy analysis of cell doublet and aggregate frequency in our single-cell samples, observed Iridium DNA intercalator levels consistent with phagocytosis rather than cell doublets or aggregates, and used our mass-tag cell barcoding scheme to remove cell doublets and aggregates from our analysis^[45]. That said, we cannot rule out the possibility that some fraction of our observed putative phagocytosing glia are in fact cell doublets or aggregates that made it through these stringency filters. Additional mass cytometry experiments using markers of phagocytosis such as Jedi1, MEGF10, and CD68 could improve our interpretation of these results, but commercially available antibodies against Jedi1 and MEGF10 have not been validated for flow cytometry or mass cytometry, and anti-CD68 antibodies are not directly compatible with the methanol permeabilization step used in this study. As the frequency of phagocytosing SGCs is expected to drop in adulthood with macrophage infiltration, analysis of adult tissues could serve as a negative control for cell doublets and aggregates, but we have not yet optimized our dissection and cell dissociation protocols to isolate adult DRG cells with high yield. Future experiments with IHC or imaging mass cytometry (IMC)^[140] and multiplexed ion beam imaging (MIBI)^[143] could shed further light on these questions, and represent a highly complementary approach to the mass cytometry techniques employed here.

In this study, we identified statistically significant sex-specific differences in abundance across all major subsets of neuronal populations using mass cytometry, but there are three important caveats to consider for this approach. (1) The use of a 40-marker panel may not be sufficient to identify every subset of DRG cell populations, although previous mass cytometry analysis identified DRG cell populations at a level comparable to scRNA-seq^[45]. (2) The digestive enzymes used for cell dissociation, particularly trypsin, will cleave proteins on the cell surface, and may alter the cell surface marker profile in comparison to native, undigested cells. (3) Changes in relative abundance for one cell type may be caused by large changes in another

cell type (zero-sum), rather than different absolute numbers for the cell type of interest. (4) The potential for systematic bias in the cell types recovered after preparation for mass cytometry may not be uniform. To address caveats 3 and 4, we have applied the orthogonal technique of immunofluorescence microscopy to corroborate our results. All microscopy tests that we performed have validated our mass cytometry results, but the limited number of fluorophores which can be used simultaneously limits the precision in cell type subsets that we can validate by immunofluorescence microscopy.

In summary, our analysis of sexual dimorphism within neuronal and glial populations in the DRG at P0 has highlighted the power of mass cytometry to examine both dramatic and subtle cell type differences between sexes. Additionally, this work has laid the foundation for future studies to further explore the impact of sex on DRG development and function through examining the role of developmental inflammation on population abundance, investigating the appearance and progression of sexually dimorphic cell types throughout embryonic and postnatal development and then into adulthood, and bridging the gap between abundance and function through analysis of electrical activity or signaling.

Chapter 3: Conclusions and Future Directions

3.1 Future Directions

3.1.1 Examining Sexual Dimorphism

There are two potential explanations for the sex differences we found in some neuronal populations at postnatal day 0 – (1) there is a fundamental difference between males and females in the abundance and/or type of somatosensory neurons produced, or (2) the same abundance and/or cell types will be produced, but the timing differs between sexes. One way to gain a better understanding of how sex impacts the molecular development of different cell populations in the DRG is to examine differences over time. Conducting a time course study in which we begin at an early embryonic period and examine the abundance and composition of different cell types through adulthood would assist in answering a few specific questions. (1) When does sexual dimorphism in molecular characterization and abundance of specific cell populations begin and potentially end? (2) Is sexual dimorphism present in all cell types throughout the mouse's lifespan? (3) Do molecularly distinct cell populations exist in one sex but not the other? (4) Are there differences in the rate of maturation for specific cell types? Being able to conduct a time course study could provide valuable insight into the “who” (in which cell populations) and “when” (during which periods of development) of sexual dimorphism in the DRG.

One gap in my work examining sex differences in cell type abundance and characterization is an understanding of what might be contributing to the sex differences we observed. Although there are studies that have already highlighted the importance of hormones in DRG neuronal response^[119], it would also be interesting to examine the molecular impact of hormones on

development and maturation of different cell types. A study in which mice are “masculinized” or “feminized” could be conducted to see if the differences in cell abundance and molecular properties could be artificially generated through changes in hormone levels or hormone receptor responsiveness^[77,119,134,135]. Additionally, if hormones cannot explain the sex differences in abundance and population characterization, we could then begin experimenting with other scenarios that might be contributing to the observed effect.

Examination of sex-separated DRGs in a time course study and analysis of DRGs from mice that have had their hormone receptor expression or circulating levels altered can be well studied using mass cytometry. Although mass cytometry is a powerful tool for examining the molecular composition of cells in a high throughput manner, it is not a suitable technique for answering all of the questions associated with sexual dimorphism in the DRG. Along with behavioral experiments which will be further discussed below, utilizing cell cultures could prove another valuable method for examining how hormones can impact development of neuronal and glial populations. By culturing primary neuronal cells or neuron-like immortal cell lines, for example, PC12 cells, excess androgens and/or estrogens could be added to the culture to assess how factors such as survival, or marker expression are altered. Although *in vitro* methods have the disadvantage of being removed from their natural environment and thus not an exact match for the true physiological environment, they have the benefit of much more control. This can lead to a much more basic understanding of what factors, in this case sex hormone levels, can directly impact specific and distinct cell types.

In addition to sex hormone levels, cell intrinsic differences driven by the presence of X and Y chromosomes, could also be contributing to sex differences in cell population differentiation and development. In females, the presence of two X chromosomes normally does not result in a “double-dose” of X genes as one of the X chromosomes is usually inactivated^[136]. Although

infrequent, occasional instances by which the second X chromosome in females is not inactivated have occurred which could impact gene expression in those cells^[137]. Additionally, whether or not the paternal or maternal X chromosome is inactivated in females might also drive sexual dimorphism in gene expression between males and females^[138]. Although this does provide another interesting angle to examine, the ability of gonadal hormones to fully reverse phenotypes observed in the opposite sex imply a much stronger connection between sexual dimorphism and hormonal differences than sexual dimorphism and sex chromosome gene expression^[119,138,139].

Overall, there are multiple different approaches that should be used to gain a deeper understanding of sexual dimorphism in cell type characterization and abundance in the DRG. More studies should be conducted to elucidate what cell populations show sex differences and during what time periods do those differences emerge or terminate. Additionally, further investigation of the role of sex hormones and sex chromosomes on cell development and maturation could provide a clearer explanation for the underlying drivers of these differences.

3.1.2 Mass Cytometry of Developing and Adult DRG

The use of mass cytometry to examine protein-level expression levels of roughly 40 different markers within individual cells is incredibly powerful and invaluable to gaining a more complete picture of the molecular composition of different cell populations. Although mass cytometry has many advantages, there are limitations to the technique as well.

Currently, examining neural tissues and cells is new for mass cytometry. Traditionally, mass cytometry is used primarily for immune cell characterization. Although our lab was able to develop a technique for preparation and examination of neural cells by mass cytometry, it has

found that some additional properties of neural cells make them more problematic than immune cells for this approach. One such property is myelin. The amount of myelin present around axons tends to increase as the mouse develops. Myelin is generally wrapped around axons and has a tendency to attach to other cells nearby when dissociated. This presents an issue in which the tissue can either not be properly dissociated leading to many clumps that will have to be excluded from analysis or it could so closely attach to a single-cell that it could alter the detection of marker expression on that cell. Because of the issue presented by large amounts of myelin, all studies to date conducted in our lab have solely used embryonic or early postnatal neural tissue to reduce the amount of myelin present. Although this is sufficient when aiming to examine developmental time periods, it poses a problem if investigating adulthood is ever necessary or of interest.

To assess protein expression in a high throughput manner in adulthood using mass cytometry there are currently two main options. The first option is to find a way to optimize the protocol to try to reduce the ill-effects of increased myelination in the dissociation and marker detection process. This could be done by trying to remove as much of the nerve root as possible from the DRG before beginning the dissociation process and then trying methods to remove myelin from samples such as a Percoll gradient. Another option would be to use an adaptation of mass cytometry known as imaging mass cytometry (IMC). IMC is like a combination of mass cytometry and immunohistochemistry (IHC). Thin sections of tissue are sliced, placed on a slide, and stained with metal-labeled antibodies. An IMC device is then used to scan over and laser ablate a section of the tissue. The released metal ions are then detected, somewhat similarly to mass cytometry, while keeping the spatial information intact^[140,141]. The ability to maintain spatial information is incredibly valuable for helping to understand the molecular composition of cells that are near each other or have a particular arrangement within the DRG. Additionally, it can provide a simpler way to examine adult tissues as the confounds of increased myelin would be

irrelevant. Although there are limitations to this technique as well, it could prove a valuable future direction in not only being able to examine protein-level expression in neural tissue from older animals, but also better characterizing the differences in marker expression that might exist spatially.

3.1.3 Further Examination of All Cell Populations in the DRG

One of the findings from my work showed sexual dimorphism in endothelial cells. Because of the markers used in our panel, we were only able to identify these cells with a few markers, but did not have the ability to explore the sexual dimorphism in these populations more specifically beyond this broad characterization. Similarly, although no sexual dimorphism was observed in leukocytes and macrophages, having a more specialized panel to further characterize any potential subpopulation differences would be valuable.

Our characterization of glial cells and neuronal populations did highlight sexual dimorphism that existed within multiple distinct subpopulations. Although we were able to identify many specific subpopulations at this time point, the ability to examine even more specialized cell types would be invaluable. For example, one commonly studied subtype of nociceptors in the DRG are TrpV1+ neurons that are sensitive to certain temperature ranges of heat as well as chemicals such as capsaicin. As this marker was not included in our panel, we were unable to examine sexual dimorphism that might exist within this specific subtype of nociceptive neurons. In addition to limitations within our neuronal populations, we were also limited in the specificity we were able to achieve within our glial cell types. As Schwann cells are either myelinating or non-myelinating, having the appropriate markers to examine sexual dimorphism in these subtypes would be a valuable future direction. For the satellite glial cells, this is less of an issue as most

observed differences in marker expression between SGC subtypes would likely be in relation to maturity and not distinct subpopulations.

Not only will future studies need to have more thorough and tailored panels to be able to better identify specific subpopulations for the main cell types present within the DRG, there will also need to be a more thorough investigation of maturational state. In our work, we found a decrease in expression of MAP2 in females, a marker typically found in more mature neurons in the DRG. The ability to assess maturational states by expression level could be further accentuated by examining expression of markers known to only appear for transient time periods during development. If combined with a time course study, this could provide some interesting insight into the rate of development for specific cell populations.

One limitation of mass cytometry is the biased and somewhat limited nature of possible protein detection. Although 40 markers is much more than most other protein-level approaches can theoretically reach, it is not a completely unbiased approach to examining protein expression. For specific regions that are more homogenous and don't have a multitude of different cell types with overlapping expression profiles, this approach works well. The DRG fits that description well, however, this technique may prove to be more limiting for other regions like the brain which have much higher levels of cellular diversity. The panel of approximately 40 different molecular markers you want to use can be tailored to answer specific questions, but it is important to note that mass cytometry does require some knowledge of the marker expression you expect to see. Along with designing a panel of markers that fits the specific question being asked, validation of the antibodies is required. The specificity and efficiency of labeling can vary widely between antibodies. To ensure no alterations to binding are introduced when metal labeling an antibody and that the proper populations of cells are being analyzed, a thorough process of validation is required. Future work in the lab will aim to expand the antibodies possible for use in mass

cytometry and thus work toward developing panels of antibodies that are tailored for specific tissues or systems.

In addition to further defining more distinct cell subtypes through use of mass cytometry, additional techniques should be used to corroborate our findings. For our manuscript, we used immunohistochemistry (IHC) to compare sex differences observed at P0 by mass cytometry with those collected by IHC. Although it is unlikely to see precise alignment in the percentage of total cell populations between these two techniques, it does allow us to examine if our data is trending in similar directions. Additionally, IHC can also be used to reduce concerns about cell loss and systematic bias during dissociation (as discussed in section 3.1.2). For our study, we found that the trends in sexual dimorphism for the neuronal populations seen by mass cytometry were similar to those observed by IHC, but this would need to be done for all cell types and ideally for some of the stronger differences observed in more specific subpopulations.

Overall, future studies should use more specialized panels to further characterize different cell populations and delineate between specific population subtypes. This could allow for a more specific description of sex differences in cell type abundance. Additionally, the trends observed with mass cytometry should be further corroborated by additional techniques like IHC or even flow-cytometry.

3.1.4 Connecting Molecular Characterization with Cellular Function

In our study, we were able to identify differences in relative abundance between different cell populations, but we were unable to connect these changes in relative abundance to functional differences. Future studies could bridge this gap in a multitude of ways, but two potential options

are (1) through examination of behavioral differences and (2) by investigating changes in neuronal signaling after activation.

Behavioral studies can be a valuable tool for determining if the observed sex differences in the relative abundance of neuronal populations actually result in a functional difference in the response of the mouse. A few different behavioral tests can be useful for assessing sensitivity to painful stimuli that target some neuronal subtypes in the DRG. The hot plate test, which involves placing a mouse on a heat block and recording the latency in time it takes them to remove their paw, targets some of the thermosensitive nociceptors in the DRG. The Von Frey test, which involves poking a mouse's hind paw with filaments of increasing force and determining when or how frequently a response to the filament occurs, targets some of the mechanosensitive neuronal populations. For the proprioceptive neuronal populations, a behavioral test like the rotarod test should partially target proprioceptive populations in the DRG. In the rotarod test, a mouse is placed on a rotating rod that increases in acceleration as time progresses and the latency in the time it takes to fall off of the rod is recorded. However, for most of these behavioral tests, and most behavioral studies in general, they are optimized and almost exclusively conducted on adult mice. Examination of primarily adult mice is done for a variety of reasons, but for examining the connection between relative abundance of neuronal populations and functional changes in mouse behavior of very young mice, the ability to conduct behavioral tests in pups is a necessity. To address this void in behavioral techniques, I developed a series of behavioral assays modeled after the hot plate, Von Frey, and rotarod tests to examine behavior in early postnatal pups. These behavioral assays essentially rely on the reflexes that begin developing in pups from very early postnatal ages and could serve as a way to determine if behavior is impacted by sex differences at this early age (Figure 20a).

As a pilot study, I used WT and tumor necrosis factor receptor 1 knockout (TNFR1^{-/-}) animals to determine if differences in behavior were observed at postnatal day 4. The results show that there does seem to be an increased sensitivity of the TNFR1^{-/-} pups in the overall percentage of tactile response when using the 1g Von Frey filament. Although no other significant results are found in the current data, increasing the sample size is necessary for accurate examination of differences between these two groups (Figure 20b). Overall, the development of these behavioral tests for young pups could be invaluable for connecting differences seen in cell type abundances or molecular profiles during early development to differences in animal behavior.

Figure 20

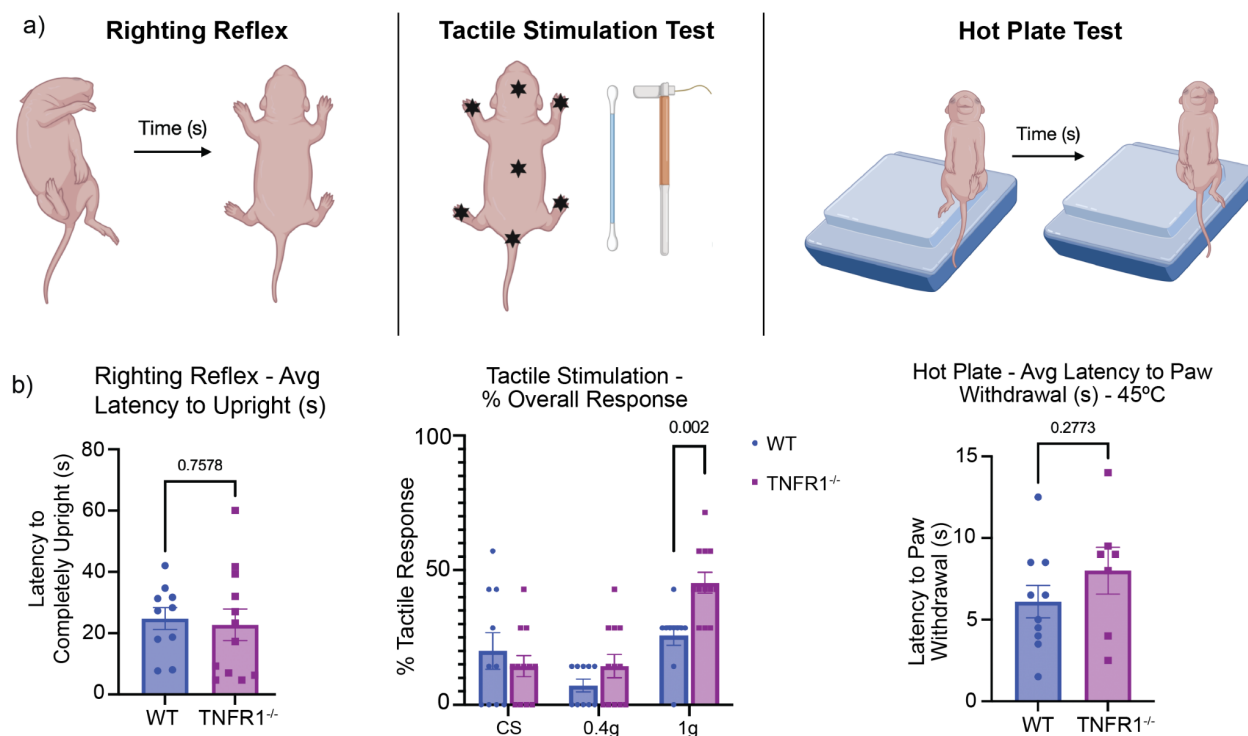


Figure 20: **Behavioral assays in early postnatal pups and pilot data with TNFR1^{-/-} pups.** a) Schematic depicting the righting reflex test, tactile stimulation test, and hot plate test. The righting reflex test works by tapping into a mouse pup's reflexive desire to not be on its back, but

rather on its stomach. This test works by flipping a pup onto its back and then measuring the latency to flip back over to its stomach. It could be used as an imperfect measurement for proprioception which relates to one's body positioning in space. The tactile stimulation test works by using a cotton swab or Von Frey filaments corresponding to different amounts of applied force and tapping the pup on different areas on its body, including the head, forepaws, back, hind paws, and tail base. Anytime the mouse reacts to the stimulus, you record that as a response. You can then calculate the percentage of times the mouse responds to each of the seven presentations of the stimulus. This could be an imperfect measurement of mechanoreception as well as nociception. The hot plate test using a hot plate set to a noxious temperature. While holding the pup, you place one of its hind paws on the hot plate and then measure how long it takes them to lift it off of the hot plate. This test is an imperfect way to measure nociception specifically targeting thermoreceptors. **b)** These graphs represent pilot data collected from P4 WT and TNFR1^{-/-} pups that were put through the righting reflex test, tactile stimulation test, and hot plate test. No significant differences were found between WT and TNFR1^{-/-} pups in the righting reflex test, hot plate test, or 2 or the 3 stimuli used for the tactile stimulation test. However, even with an inadequate sample size, we still see a significant difference in sensitivity to the 1g force Von Frey filament between the two genotypes. This is only preliminary data and will require an increased sample size and further validation of the behavioral assays before firm conclusions can be drawn.

In addition to assessing alterations in animal behavior, it is important to determine the connection between cell population abundance and firing ability and sensitivity of the neuronal populations present in the developing DRG. Electrophysiology is one way to assess firing rate in particular, but for pups this small, doing patch clamp recordings in a slice would likely be difficult. A few other potential options for assessing functioning of neuronal populations would be culturing cells from pups and adding known stimulants such as capsaicin or menthol to these

primary neuronal cultures. Through fluorescent calcium imaging, you could assess if the abundance of neurons present within a specific area, or the presence or absence of varying densities of satellite glial cells, impacts the firing ability of these specific neuronal populations. Similarly, assessing changes in signaling through either more high throughput mechanisms, like flow or mass cytometry that target phosphorylated proteins, or more quick and common techniques like Western Blots, could provide insight to alterations to signaling that might be occurring in our different neuronal populations. One benefit of using mass cytometry in this manner, is the ability to use multiple markers to identify specific populations, while also using markers that target phosphorylated signaling proteins, thus giving you a much more complete picture of which specific cell populations are functionally active or responding to a specific stimuli.

3.2 Conclusions

My published study examining sexual dimorphism in the DRG at P0 found that specifically within neuronal populations, sex differences do exist. Overall, females seemed to have a higher relative abundance of neurons in general, with specific increases in TrkB⁺ and TrkC⁺ neurons. Males had a higher relative abundance of TrkA⁺ neurons at this time point. In addition to differences in neuronal abundance, there also seemed to be an increase in the percentage of female neurons that were low in more mature neuronal markers such as MAP2, which was confirmed by pseudotime analysis. Additionally, we saw sex differences in the debris consumed by phagocytosing glia that aligned with sex differences in neuronal abundance.

This published study highlighted the value of examining sex differences with high dimensional analysis tools like mass cytometry. Although there were limitations that future experiments will

likely address, this work also raises additional questions that later studies can explore. Future studies will likely investigate (1) when sexual dimorphism in the DRG begins and potentially ends with a time course study, (2) potential sex differences in the cell populations that arise and mature in the DRG, (3) the ability of adult neural tissue to be examined by mass cytometry or other methods, (4) enhanced characterization and exploration of sex differences for all cell types, but specifically cell populations that were not studied in depth in my work, and (5) the prospect of connecting abundance differences determined by mass cytometry to functional differences assessed by behavioral or signaling assays.

My project along with the work of Austin Keeler^[45] and Amy Van Deusen^[142] have laid the foundations for the possibilities associated with using mass cytometry to characterize and assess neural cells, however, there is still more optimization required to fully utilize the power of this technique. With enhanced antibody panels, the addition of signaling molecules, and the complement of other techniques to corroborate and expound upon discoveries made by mass cytometry, this tool could prove invaluable for quickly and robustly examining multiple cell populations in neural tissues and beyond.

References

1. Kaas, J.H. (2012). Somatosensory System. In *The human nervous system* (Elsevier), pp. 1074–1109.
2. Emery, E.C., and Ernfors, P. (2018). Dorsal root ganglion neuron types and their functional specialization. In *The oxford handbook of the neurobiology of pain*, J. N. Wood, ed. (Oxford University Press).
3. Lopes, D.M., Denk, F., and McMahon, S.B. (2017). The molecular fingerprint of dorsal root and trigeminal ganglion neurons. *Front. Mol. Neurosci.* 10, 304.
4. Dupin, E., Creuzet, S., and Le Douarin, N.M. (2006). The contribution of the neural crest to the vertebrate body. *Adv. Exp. Med. Biol.* 589, 96–119.
5. Sela-Donenfeld, D., and Kalcheim, C. (2000). Inhibition of noggin expression in the dorsal neural tube by somitogenesis: a mechanism for coordinating the timing of neural crest emigration. *Development*.
6. Savagner, P. (2001). Leaving the neighborhood: molecular mechanisms involved during epithelial-mesenchymal transition. *Bioessays* 23, 912–923.
7. Wegner, M., and Stolt, C.C. (2005). From stem cells to neurons and glia: a Soxist's view of neural development. *Trends Neurosci.* 28, 583–588.
8. Lallemand, F., and Ernfors, P. (2012). Molecular interactions underlying the specification of sensory neurons. *Trends Neurosci.* 35, 373–381.
9. Abaira, V.E., and Ginty, D.D. (2013). The sensory neurons of touch. *Neuron* 79, 618–639.
10. Crawford, L.K., and Caterina, M.J. (2020). Functional anatomy of the sensory nervous system: updates from the neuroscience bench. *Toxicol. Pathol.* 48, 174–189.
11. Klein, R. (1994). Role of neurotrophins in mouse neuronal development. *FASEB J.* 8,

- 738–744.
12. Lindsay, R.M. (1996). Role of neurotrophins and trk receptors in the development and maintenance of sensory neurons: an overview. *Philos. Trans. R. Soc. Lond. B Biol. Sci.* *351*, 365–373.
 13. Moqrigh, A., Earley, T.J., Watson, J., Andahazy, M., Backus, C., Martin-Zanca, D., Wright, D.E., Reichardt, L.F., and Patapoutian, A. (2004). Expressing TrkC from the TrkA locus causes a subset of dorsal root ganglia neurons to switch fate. *Nat. Neurosci.* *7*, 812–818.
 14. Fritz, N., Illert, M., de la Motte, S., Reeh, P., and Saggau, P. (1989). Pattern of monosynaptic Ia connections in the cat forelimb. *J Physiol (Lond)* *419*, 321–351.
 15. Lüscher, H.R., and Clamann, H.P. (1992). Relation between structure and function in information transfer in spinal monosynaptic reflex. *Physiol. Rev.* *72*, 71–99.
 16. Mears, S.C., and Frank, E. (1997). Formation of specific monosynaptic connections between muscle spindle afferents and motoneurons in the mouse. *J. Neurosci.* *17*, 3128–3135.
 17. Usoskin, D., Furlan, A., Islam, S., Abdo, H., Lönnerberg, P., Lou, D., Hjerling-Leffler, J., Haeggström, J., Kharchenko, O., Kharchenko, P.V., *et al.* (2015). Unbiased classification of sensory neuron types by large-scale single-cell RNA sequencing. *Nat. Neurosci.* *18*, 145–153.
 18. Ochoa, J., and Torebjörk, E. (1983). Sensations evoked by intraneural microstimulation of single mechanoreceptor units innervating the human hand. *J Physiol (Lond)* *342*, 633–654.
 19. Woodbury, C.J., and Koerber, H.R. (2007). Central and peripheral anatomy of slowly adapting type I low-threshold mechanoreceptors innervating trunk skin of neonatal mice. *J. Comp. Neurol.* *505*, 547–561.

20. Andrew, D. (2010). Quantitative characterization of low-threshold mechanoreceptor inputs to lamina I spinoparabrachial neurons in the rat. *J Physiol (Lond)* 588, 117–124.
21. Nagi, S.S., and Mahns, D.A. (2013). Mechanical allodynia in human glabrous skin mediated by low-threshold cutaneous mechanoreceptors with unmyelinated fibres. *Exp. Brain Res.* 231, 139–151.
22. Olson, W., Dong, P., Fleming, M., and Luo, W. (2016). The specification and wiring of mammalian cutaneous low-threshold mechanoreceptors. *Wiley Interdiscip. Rev. Dev. Biol.* 5, 389–404.
23. Sherman, D.L., and Brophy, P.J. (2005). Mechanisms of axon ensheathment and myelin growth. *Nat. Rev. Neurosci.* 6, 683–690.
24. Morris, J.K., Lin, W., Hauser, C., Marchuk, Y., Getman, D., and Lee, K.F. (1999). Rescue of the cardiac defect in ErbB2 mutant mice reveals essential roles of ErbB2 in peripheral nervous system development. *Neuron* 23, 273–283.
25. Woodhoo, A., and Sommer, L. (2008). Development of the Schwann cell lineage: from the neural crest to the myelinated nerve. *Glia* 56, 1481–1490.
26. Jessen, K.R., and Mirsky, R. (2005). The origin and development of glial cells in peripheral nerves. *Nat. Rev. Neurosci.* 6, 671–682.
27. Finzsch, M., Schreiner, S., Kichko, T., Reeh, P., Tamm, E.R., Bösl, M.R., Meijer, D., and Wegner, M. (2010). Sox10 is required for Schwann cell identity and progression beyond the immature Schwann cell stage. *J. Cell Biol.* 189, 701–712.
28. Ma, K.H., and Svaren, J. (2018). Epigenetic control of schwann cells. *Neuroscientist* 24, 627–638.
29. Jessen, K.R., and Mirsky, R. (2019). Schwann cell precursors; multipotent glial cells in embryonic nerves. *Front. Mol. Neurosci.* 12, 69.

30. Feltri, M.L., Graus Porta, D., Previtali, S.C., Nodari, A., Migliavacca, B., Cassetti, A., Littlewood-Evans, A., Reichardt, L.F., Messing, A., Quattrini, A., *et al.* (2002). Conditional disruption of beta 1 integrin in Schwann cells impedes interactions with axons. *J. Cell Biol.* *156*, 199–209.
31. Charles, P., Reynolds, R., Seilhean, D., Rougon, G., Aigrot, M.S., Niezgoda, A., Zalc, B., and Lubetzki, C. (2002). Re-expression of PSA-NCAM by demyelinated axons: an inhibitor of remyelination in multiple sclerosis? *Brain* *125*, 1972–1979.
32. Chan, J.R., Watkins, T.A., Cosgaya, J.M., Zhang, C., Chen, L., Reichardt, L.F., Shooter, E.M., and Barres, B.A. (2004). NGF controls axonal receptivity to myelination by Schwann cells or oligodendrocytes. *Neuron* *43*, 183–191.
33. Milosavljević, A., Jančić, J., Mirčić, A., Dožić, A., Boljanović, J., Milisavljević, M., and Četković, M. (2021). Morphological and functional characteristics of satellite glial cells in the peripheral nervous system. *Folia Morphol (Warsz)* *80*, 745–755.
34. Schon, F., and Kelly, J.S. (1974). Autoradiographic Localisation of [³H]GABA and [³H]Glutamate Over Satellite Glial Cells. *Brain Res.*
35. Hosli, E., and Hosli, L. (1977). Autoradiographic Localization of the Uptake of [3H]GABA and [3H] L-Glutamic Acid in Neurones and Glial Cells of Cultured Dorsal Root Ganglia. *Neurosci Lett.*
36. Gola, M., Niel, J.P., Delmas, P., and Jacquet, G. (1993). Satellite glial cells in situ within mammalian prevertebral ganglia express K⁺ channels active at rest potential. *J. Membr. Biol.* *136*, 75–84.
37. Cherkas, P.S., Huang, T.-Y., Pannicke, T., Tal, M., Reichenbach, A., and Hanani, M. (2004). The effects of axotomy on neurons and satellite glial cells in mouse trigeminal ganglion. *Pain* *110*, 290–298.

38. Konishi, T. (1996). Developmental and activity-dependent changes in K⁺ currents in satellite glial cells in mouse superior cervical ganglion. *Brain Res.* 708, 7–15.
39. Tang, B.L. (2019). Why is NMNAT Protective against Neuronal Cell Death and Axon Degeneration, but Inhibitory of Axon Regeneration? *Cells* 8.
40. Wu, H.-H., Bellmunt, E., Scheib, J.L., Venegas, V., Burkert, C., Reichardt, L.F., Zhou, Z., Fariñas, I., and Carter, B.D. (2009). Glial precursors clear sensory neuron corpses during development via Jedi-1, an engulfment receptor. *Nat. Neurosci.* 12, 1534–1541.
41. Buss, R.R., Sun, W., and Oppenheim, R.W. (2006). Adaptive roles of programmed cell death during nervous system development. *Annu. Rev. Neurosci.* 29, 1–35.
42. Deppmann, C.D., Mihalas, S., Sharma, N., Lonze, B.E., Niebur, E., and Ginty, D.D. (2008). A model for neuronal competition during development. *Science* 320, 369–373.
43. Fariñas, I., Yoshida, C.K., Backus, C., and Reichardt, L.F. (1996). Lack of neurotrophin-3 results in death of spinal sensory neurons and premature differentiation of their precursors. *Neuron* 17, 1065–1078.
44. Costa, F.A.L., and Neto, F.L.M. (2015). Satellite glial cells in sensory ganglia: its role in pain. *Brazilian Journal of Anesthesiology (English Edition)* 65, 73–81.
45. Keeler, A.B., Van Deusen, A.L., Gadani, I.C., Williams, C.M., Goggin, S.M., Hirt, A.K., Vradenburgh, S.A., Fread, K.I., Puleo, E.A., Jin, L., *et al.* (2022). A developmental atlas of somatosensory diversification and maturation in the dorsal root ganglia by single-cell mass cytometry. *Nat. Neurosci.* 25, 1543–1558.
46. Hanani, M. (2005). Satellite glial cells in sensory ganglia: from form to function. *Brain Res. Brain Res. Rev.* 48, 457–476.
47. SUGIMURA, K., HAIMOTO, H., NAGURA, H., KATO, K., and TAKAHASHI, Ak. (1989). Immunohistochemical Differential Distribution of S100a and S100b in the Peripheral

Nervous System of the Rat. Muscle Nerve.

48. Nascimento, R.S., Santiago, M.F., Marques, S.A., Allodi, S., and Martinez, A.M.B. (2008). Diversity among satellite glial cells in dorsal root ganglia of the rat. *Braz. J. Med. Biol. Res.* *41*, 1011–1017.
49. Hanani, M., and Spray, D.C. (2020). Emerging importance of satellite glia in nervous system function and dysfunction. *Nat. Rev. Neurosci.* *21*, 485–498.
50. Mapps, A.A., Thomsen, M.B., Boehm, E., Zhao, H., Hattar, S., and Kuruvilla, R. (2022). Diversity of satellite glia in sympathetic and sensory ganglia. *Cell Rep.* *38*, 110328.
51. Schena, M., Shalon, D., Davis, R.W., and Brown, P.O. (1995). Quantitative Monitoring of Gene Expression Patterns with a Complementary DNA Microarray. *Science*.
52. Lashkari, D.A., DeRisi, J.L., McCusker, J.H., Namath, A.F., Gentile, C., Hwang, S.Y., Brown, P.O., and Davis, R.W. (1997). Yeast microarrays for genome wide parallel genetic and gene expression analysis. *Proc Natl Acad Sci USA* *94*, 13057–13062.
53. Kurimoto, K., Yabuta, Y., Ohinata, Y., Ono, Y., Uno, K.D., Yamada, R.G., Ueda, H.R., and Saitou, M. (2006). An improved single-cell cDNA amplification method for efficient high-density oligonucleotide microarray analysis. *Nucleic Acids Res.* *34*, e42.
54. Esumi, S., Wu, S.-X., Yanagawa, Y., Obata, K., Sugimoto, Y., and Tamamaki, N. (2008). Method for single-cell microarray analysis and application to gene-expression profiling of GABAergic neuron progenitors. *Neurosci. Res.* *60*, 439–451.
55. Ozsolak, F., Platt, A.R., Jones, D.R., Reifemberger, J.G., Sass, L.E., McInerney, P., Thompson, J.F., Bowers, J., Jarosz, M., and Milos, P.M. (2009). Direct RNA sequencing. *Nature* *461*, 814–818.
56. Tang, F., Barbacioru, C., Wang, Y., Nordman, E., Lee, C., Xu, N., Wang, X., Bodeau, J., Tuch, B.B., Siddiqui, A., *et al.* (2009). mRNA-Seq whole-transcriptome analysis of a single

- cell. *Nat. Methods* 6, 377–382.
57. Islam, S., Kjällquist, U., Moliner, A., Zajac, P., Fan, J.-B., Lönnerberg, P., and Linnarsson, S. (2011). Characterization of the single-cell transcriptional landscape by highly multiplex RNA-seq. *Genome Res.* 21, 1160–1167.
 58. Chiu, I.M., Barrett, L.B., Williams, E.K., Strohlic, D.E., Lee, S., Weyer, A.D., Lou, S., Bryman, G.S., Roberson, D.P., Ghasemlou, N., *et al.* (2014). Transcriptional profiling at whole population and single cell levels reveals somatosensory neuron molecular diversity. *eLife* 3.
 59. Smith-Anttila, C.J.A., Mason, E.A., Wells, C.A., Aronow, B.J., Osborne, P.B., and Keast, J.R. (2020). Identification of a sacral, visceral sensory transcriptome in embryonic and adult mice. *eNeuro* 7.
 60. Sharma, N., Flaherty, K., Lezgiyeva, K., Wagner, D.E., Klein, A.M., and Ginty, D.D. (2020). The emergence of transcriptional identity in somatosensory neurons. *Nature* 577, 392–398.
 61. Tasdemir-Yilmaz, O.E., Druckenbrod, N.R., Olukoya, O.O., Dong, W., Yung, A.R., Bastille, I., Pazyra-Murphy, M.F., Sitko, A.A., Hale, E.B., Vigneau, S., *et al.* (2021). Diversity of developing peripheral glia revealed by single-cell RNA sequencing. *Dev. Cell* 56, 2516-2535.e8.
 62. Ibberson, D., Benes, V., Muckenthaler, M.U., and Castoldi, M. (2009). RNA degradation compromises the reliability of microRNA expression profiling. *BMC Biotechnol.* 9, 102.
 63. Houseley, J., and Tollervey, D. (2009). The many pathways of RNA degradation. *Cell* 136, 763–776.
 64. Anderson, L., and Seilhamer, J. (1997). A comparison of selected mRNA and protein abundances in human liver. *Electrophoresis* 18, 533–537.

65. Anderson, N.L., and Anderson, N.G. (1998). Proteome and proteomics: new technologies, new concepts, and new words. *Electrophoresis* 19, 1853–1861.
66. Gygi, S.P., Rochon, Y., Franza, B.R., and Aebersold, R. (1999). Correlation between protein and mRNA abundance in yeast. *Mol. Cell. Biol.* 19, 1720–1730.
67. Futcher, B., Latter, G.I., Monardo, P., McLaughlin, C.S., and Garrels, J.I. (1999). A sampling of the yeast proteome. *Mol. Cell. Biol.* 19, 7357–7368.
68. Pradet-Balade, B., Boulmé, F., Beug, H., Müllner, E.W., and Garcia-Sanz, J.A. (2001). Translation control: bridging the gap between genomics and proteomics. *Trends Biochem Sci.*
69. Marshall, R.S., and Vierstra, R.D. (2019). Dynamic regulation of the 26S proteasome: from synthesis to degradation. *Front. Mol. Biosci.* 6, 40.
70. Bonner, W.A., Hulett, H.R., Sweet, R.G., and Herzenberg, L.A. (1972). Fluorescence activated cell sorting. *Rev. Sci. Instrum.* 43, 404–409.
71. Herzenberg, L.A., Parks, D., Sahaf, B., Perez, O., Roederer, M., and Herzenberg, L.A. (2002). The history and future of the fluorescence activated cell sorter and flow cytometry: a view from Stanford. *Clin. Chem.* 48, 1819–1827.
72. Bandura, D.R., Baranov, V.I., Ornatsky, O.I., Antonov, A., Kinach, R., Lou, X., Pavlov, S., Vorobiev, S., Dick, J.E., and Tanner, S.D. (2009). Mass cytometry: technique for real time single cell multitarget immunoassay based on inductively coupled plasma time-of-flight mass spectrometry. *Anal. Chem.* 81, 6813–6822.
73. Bendall, S.C., Simonds, E.F., Qiu, P., Amir, E.D., Krutzik, P.O., Finck, R., Bruggner, R.V., Melamed, R., Trejo, A., Ornatsky, O.I., *et al.* (2011). Single-cell mass cytometry of differential immune and drug responses across a human hematopoietic continuum. *Science* 332, 687–696.

74. Blanco, G., Diaz, H., Carrer, H.F., and Beaugé, L. (1990). Differentiation of rat hippocampal neurons induced by estrogen in vitro: effects on neuritogenesis and Na, K-ATPase activity. *J. Neurosci. Res.* 27, 47–54.
75. Krebs-Kraft, D.L., Hill, M.N., Hillard, C.J., and McCarthy, M.M. (2010). Sex difference in cell proliferation in developing rat amygdala mediated by endocannabinoids has implications for social behavior. *Proc Natl Acad Sci USA* 107, 20535–20540.
76. Carrer, H.F., Cambiasso, M.J., and Gorosito, S. (2005). Effects of estrogen on neuronal growth and differentiation. *J. Steroid Biochem. Mol. Biol.* 93, 319–323.
77. McCarthy, M.M. (2008). Estradiol and the developing brain. *Physiol. Rev.* 88, 91–124.
78. Toran-Allerand, C.D. (1976). Sex steroids and the development of the newborn mouse hypothalamus and preoptic area in vitro: implications for sexual differentiation. *Brain Res.* 106, 407–412.
79. Toran-Allerand, C.D. (1980). Sex steroids and the development of the newborn mouse hypothalamus and preoptic area in vitro. II. Morphological correlates and hormonal specificity. *Brain Res.*
80. Toran-Allerand, D., HASHIMOTO, K., GREENOUGH, W., and SALTARELLI, M. (1983). Sex steroids and the development of the newborn mouse hypothalamus and preopUc area in vitro: III. Effects of estrogen on dendritic differentiation. *Brain Res Dev Brain Res.*
81. Uchibori, M., and Kawashima, S. (1985). EFFECTS OF SEX STEROIDS ON THE GROWTH OF NEURONAL PROCESSES IN NEONATAL RAT HYPOTHALAMUS-PREOPT IC AREA AND CEREBRAL CORTEX IN PRIMARY CULTURE. *Int J Dev Neurosci.*
82. Lorenzo, A., Díaz, H., Carrer, H., and Cáceres, A. (1992). Amygdala neurons in vitro: neurite growth and effects of estradiol. *J. Neurosci. Res.* 33, 418–435.

83. Matsumoto, A. (1991). Synaptogenic action of sex steroids in developing and adult neuroendocrine brain. *Psychoneuroendocrinology* 16, 25–40.
84. Woolley, C.S., and McEwen, B.S. (1992). Estradiol mediates fluctuation in hippocampal synapse density during the estrous cycle in the adult rat. *J. Neurosci.* 12, 2549–2554.
85. Calizo, L.H., and Flanagan-Cato, L.M. (2000). Estrogen selectively regulates spine density within the dendritic arbor of rat ventromedial hypothalamic neurons. *J. Neurosci.* 20, 1589–1596.
86. Amateau, S.K., and McCarthy, M.M. (2002). A novel mechanism of dendritic spine plasticity involving estradiol induction of prostaglandin-E2. *J. Neurosci.* 22, 8586–8596.
87. Nelson, L.H., Warden, S., and Lenz, K.M. (2017). Sex differences in microglial phagocytosis in the neonatal hippocampus. *Brain Behav. Immun.* 64, 11–22.
88. Matsumoto, A., and Arai, Y. (1983). Sex difference in volume of the ventromedial nucleus of the hypothalamus in the rat. *Endocrinol Jpn* 30, 277–280.
89. Ahern, T.H., Krug, S., Carr, A.V., Murray, E.K., Fitzpatrick, E., Bengston, L., McCutcheon, J., De Vries, G.J., and Forger, N.G. (2013). Cell death atlas of the postnatal mouse ventral forebrain and hypothalamus: effects of age and sex. *J. Comp. Neurol.* 521, 2551–2569.
90. Rhees, R.W., Shryne, J.E., and Gorski, R.A. (1990). Onset of the hormone-sensitive perinatal period for sexual differentiation of the sexually dimorphic nucleus of the preoptic area in female rats. *J. Neurobiol.* 21, 781–786.
91. Gorski, R.A. (1985). Sexual dimorphisms of the brain. *J. Anim. Sci.* 61 Suppl 3, 38–61.
92. Gorski, R., and Woodson, J. (1999). Structural sex differences in the mammalian brain: reconsidering the male/female dichotomy. In *Sexual differentiation of the brain* (CRC Press).

93. Arnold, A.P., and Gorski, R.A. (1984). Gonadal steroid induction of structural sex differences in the central nervous system. *Annu. Rev. Neurosci.* 7, 413–442.
94. Bowers, J.M., Waddell, J., and McCarthy, M.M. (2010). A developmental sex difference in hippocampal neurogenesis is mediated by endogenous oestradiol. *Biol. Sex Differ.* 1, 8.
95. Ogawa, S., Lubahn, D.B., Korach, K.S., and Pfaff, D.W. (1997). Behavioral effects of estrogen receptor gene disruption in male mice. *Proc Natl Acad Sci USA* 94, 1476–1481.
96. Ogawa, S., Chan, J., Chester, A.E., Gustafsson, J.A., Korach, K.S., and Pfaff, D.W. (1999). Survival of reproductive behaviors in estrogen receptor beta gene-deficient (betaERKO) male and female mice. *Proc Natl Acad Sci USA* 96, 12887–12892.
97. Ogawa, S., Chester, A.E., Hewitt, S.C., Walker, V.R., Gustafsson, J.A., Smithies, O., Korach, K.S., and Pfaff, D.W. (2000). Abolition of male sexual behaviors in mice lacking estrogen receptors alpha and beta (alpha beta ERKO). *Proc Natl Acad Sci USA* 97, 14737–14741.
98. Kudwa, A.E., Bodo, C., Gustafsson, J.-A., and Rissman, E.F. (2005). A previously uncharacterized role for estrogen receptor beta: defeminization of male brain and behavior. *Proc Natl Acad Sci USA* 102, 4608–4612.
99. Amateau, S.K., and McCarthy, M.M. (2004). Induction of PGE2 by estradiol mediates developmental masculinization of sex behavior. *Nat. Neurosci.* 7, 643–650.
100. Paolicelli, R.C., Bisht, K., and Tremblay, M.-È. (2014). Fractalkine regulation of microglial physiology and consequences on the brain and behavior. *Front. Cell. Neurosci.* 8, 129.
101. Patrone, C., Andersson, S., Korhonen, L., and Lindholm, D. (1999). Estrogen receptor-dependent regulation of sensory neuron survival in developing dorsal root ganglion. *Proc Natl Acad Sci USA* 96, 10905–10910.
102. Lanlua, P., Decorti, F., Gangula, P.R.R., Chung, K., Tagliatela, G., and Yallampalli, C.

- (2001). Female steroid hormones modulate receptors for nerve growth factor in rat dorsal root ganglia. *Biol. Reprod.* *64*, 331–338.
103. Sohrabji, F., Miranda, R.C., and Toran-Allerand, C.D. (1994). Estrogen differentially regulates estrogen and nerve growth factor receptor mRNAs in adult sensory neurons. *J. Neurosci.* *14*, 459–471.
104. Manson, J.E. (2010). Pain: sex differences and implications for treatment. *Metab. Clin. Exp.* *59 Suppl 1*, S16-20.
105. Bartley, E.J., and Fillingim, R.B. (2013). Sex differences in pain: A brief review of clinical and experimental findings. *Br. J. Anaesth.* *111*, 52–58.
106. Mogil, J.S. (2012). Sex differences in pain and pain inhibition: multiple explanations of a controversial phenomenon. *Nat. Rev. Neurosci.* *13*, 859–866.
107. Rosen, S., Ham, B., and Mogil, J.S. (2017). Sex differences in neuroimmunity and pain. *J. Neurosci. Res.* *95*, 500–508.
108. Sorge, R.E., and Totsch, S.K. (2017). Sex differences in pain. *J. Neurosci. Res.* *95*, 1271–1281.
109. Niesters, M., Dahan, A., Kest, B., Zacny, J., Stijnen, T., Aarts, L., and Sarton, E. (2010). Do sex differences exist in opioid analgesia? A systematic review and meta-analysis of human experimental and clinical studies. IASP.
110. Sternberg, W.F., Smith, L., and Scorr, L. (2004). Nociception and antinociception during the first week of life in mice: sex differences and test dependence. *J. Pain* *5*, 420–426.
111. Kavaliers, M., and Innes, D.G. (1990). Developmental changes in opiate-induced analgesia in deer mice: sex and population differences. *Brain Res.* *516*, 326–331.
112. Mecklenburg, J., Zou, Y., Wangzhou, A., Garcia, D., Lai, Z., Tumanov, A.V., Dussor, G.,

- Price, T.J., and Akopian, A.N. (2020). Transcriptomic sex differences in sensory neuronal populations of mice. *Sci. Rep.* 10, 15278.
113. Kim, S.J., Calejesan, A.A., Li, P., Wei, F., and Zhuo, M. (1999). Sex differences in late behavioral response to subcutaneous formalin injection in mice. *Brain Res.* 829, 185–189.
114. Banik, R.K., Woo, Y.C., Park, S.S., and Brennan, T.J. (2006). Strain and sex influence on pain sensitivity after plantar incision in the mouse. *Anesthesiology* 105, 1246–1253.
115. Lopes, D.M., Malek, N., Edey, M., Jager, S.B., McMurray, S., McMahon, S.B., and Denk, F. (2017). Sex differences in peripheral not central immune responses to pain-inducing injury. *Sci. Rep.* 7, 16460.
116. Chernov, A.V., and Shubayev, V.I. (2021). Sexual dimorphism of early transcriptional reprogramming in dorsal root ganglia after peripheral nerve injury. *Front. Mol. Neurosci.* 14, 779024.
117. Xian, F., Sondermann, J.R., Gomez Varela, D., and Schmidt, M. (2022). Deep proteome profiling reveals signatures of age and sex differences in paw skin and sciatic nerve of naïve mice. *eLife* 11.
118. Mecklenburg, J., Wangzhou, A., Hovhannisyan, A.H., Barba-Escobedo, P., Shein, S.A., Zou, Y., Weldon, K., Lai, Z., Goffin, V., Dussor, G., *et al.* (2022). Sex-dependent pain trajectories induced by prolactin require an inflammatory response for pain resolution. *Brain Behav. Immun.* 101, 246–263.
119. Luo, X., Chen, O., Wang, Z., Bang, S., Ji, J., Lee, S.H., Huh, Y., Furutani, K., He, Q., Tao, X., *et al.* (2021). IL-23/IL-17A/TRPV1 axis produces mechanical pain via macrophage-sensory neuron crosstalk in female mice. *Neuron* 109, 2691-2706.e5.
120. Reddy, L.V., Koirala, S., Sugiura, Y., Herrera, A.A., and Ko, C.P. (2003). Glial cells maintain synaptic structure and function and promote development of the neuromuscular

- junction in vivo. *Neuron* 40, 563–580.
121. Dublin, P., and Hanani, M. (2007). Satellite glial cells in sensory ganglia: their possible contribution to inflammatory pain. *Brain Behav. Immun.* 21, 592–598.
 122. Mapps, A.A., Boehm, E., Beier, C., Keenan, W.T., Langel, J., Liu, M., Thomsen, M.B., Hattar, S., Zhao, H., Tampakakis, E., *et al.* (2022). Satellite glia modulate sympathetic neuron survival, activity, and autonomic function. *eLife* 11.
 123. Smith, J.C. (2019). A review of strain and sex differences in response to pain and analgesia in mice. *Comp. Med.* 69, 490–500.
 124. Wolterink-Donselaar, I.G., Meerding, J.M., and Fernandes, C. (2009). A method for gender determination in newborn dark pigmented mice. *Lab Anim (NY)* 38, 35–38.
 125. Zunder, E.R., Finck, R., Behbehani, G.K., Amir, E.-A.D., Krishnaswamy, S., Gonzalez, V.D., Lorang, C.G., Bjornson, Z., Spitzer, M.H., Bodenmiller, B., *et al.* (2015). Palladium-based mass tag cell barcoding with a doublet-filtering scheme and single-cell deconvolution algorithm. *Nat. Protoc.* 10, 316–333.
 126. Fread, K.I., Strickland, W.D., Nolan, G.P., and Zunder, E.R. (2017). An updated debarcoding tool for mass cytometry with cell type-specific and cell sample-specific stringency adjustment. *Pac. Symp. Biocomput.* 22, 588–598.
 127. Finck, R., Simonds, E.F., Jager, A., Krishnaswamy, S., Sachs, K., Fantl, W., Pe'er, D., Nolan, G.P., and Bendall, S.C. (2013). Normalization of mass cytometry data with bead standards. *Journal of the International Society for Advancement of Cytometry.*
 128. Traag, V.A., Waltman, L., and van Eck, N.J. (2019). From Louvain to Leiden: guaranteeing well-connected communities. *Sci. Rep.* 9, 5233.
 129. Becht, E., McInnes, L., Healy, J., Dutertre, C.-A., Kwok, I.W.H., Ng, L.G., Ginhoux, F., and Newell, E.W. (2018). Dimensionality reduction for visualizing single-cell data using UMAP.

- Nat. Biotechnol. 37, 38–44.
130. McInnes, L., Healy, J., and Melville, J. (2018). UMAP: Uniform Manifold Approximation and Projection for Dimension Reduction. arXiv.
 131. Farrell, J.A., Wang, Y., Riesenfeld, S.J., Shekhar, K., Regev, A., and Schier, A.F. (2018). Single-cell reconstruction of developmental trajectories during zebrafish embryogenesis. *Science* 360.
 132. Scheib, J.L., Sullivan, C.S., and Carter, B.D. (2012). Jedi-1 and MEGF10 signal engulfment of apoptotic neurons through the tyrosine kinase Syk. *J. Neurosci.* 32, 13022–13031.
 133. Oppenheim, R.W. (1981). Neuronal cell death and some related regressive phenomena during neurogenesis: a selective historical review and progress report. *Studies in developmental neurobiology*, 74–133.
 134. Todd, B.J., Schwarz, J.M., and McCarthy, M.M. (2005). Prostaglandin-E2: a point of divergence in estradiol-mediated sexual differentiation. *Horm. Behav.* 48, 512–521.
 135. Wallen, K., and Baum, M.J. (2002). Masculinization and Defeminization in Altricial and Precocial Mammals: Comparative Aspects of Steroid Hormone Action. *Hormones, Brain and Behavior*.
 136. Lyon, M.F. (1994). X-Chromosome Inactivation. In *Molecular genetics of sex determination* (Elsevier), pp. 123–142.
 137. Carrel, L., Cottle, A.A., Goglin, K.C., and Willard, H.F. (1999). A first-generation X-inactivation profile of the human X chromosome. *Proc Natl Acad Sci USA* 96, 14440–14444.
 138. Arnold, A.P., and Burgoyne, P.S. (2004). Are XX and XY brain cells intrinsically different? *Trends Endocrinol. Metab.* 15, 6–11.

139. Nordeen, E.J., Nordeen, K.W., Sengelaub, D.R., and Arnold, A.P. (1985). Androgens Prevent Normally Occurring Cell Death in a Sexually Dimorphic Spinal Nucleus. *Science*.
140. Giesen, C., Wang, H.A.O., Schapiro, D., Zivanovic, N., Jacobs, A., Hattendorf, B., Schüffler, P.J., Grolimund, D., Buhmann, J.M., Brandt, S., *et al.* (2014). Highly multiplexed imaging of tumor tissues with subcellular resolution by mass cytometry. *Nat. Methods* 11, 417–422.
141. Chang, Q., Ornatsky, O.I., Siddiqui, I., Loboda, A., Baranov, V.I., and Hedley, D.W. (2017). Imaging Mass Cytometry. *Cytometry A* 91, 160–169.
142. Van Deusen, A.L., Goggin, S.M., Williams, C.M., Keeler, A.B., Fread, K.I., Cheng, I., Deppmann, C.D., and Zunder, E.R. (2022). A developmental atlas of the mouse brain by single-cell mass cytometry. *BioRxiv*.
143. Angelo, M., Bendall, S. C., Finck, R., Hale, M. B., Hitzman, C., Borowsky, A. D., Levenson, R. M., *et al.* (2014). Multiplexed ion beam imaging of human breast tumors. *Nature Medicine*, 20(4), 436–442.
144. Fienberg, H. G., Simonds, E. F., Fantl, W. J., Nolan, G. P. & Bodenmiller, B. (2012). A platinum-based covalent viability reagent for single-cell mass cytometry. *Cytometry A* 81, 467–475.
145. Heijink, A.M., Everts, M., Honeywell, M.E., Richards, R., Kok, Y.P., de Vries, E.G.E., Lee, M.J., and van Vugt, M.A.T.M. (2019). Modeling of Cisplatin-Induced Signaling Dynamics in Triple-Negative Breast Cancer Cells Reveals Mediators of Sensitivity. *Cell Rep.* 28, 2345-2357.e5. 10.1016/j.celrep.2019.07.070.